CEPSTRAL DECONVOLUTION METHOD FOR MEASUREMENT OF ABSORPTION AND SCATTERING COEFFICIENTS OF MATERIALS

A THESIS SUBMITTED TO
THE GRADUATE SCHOOL OF NATURAL AND APPLIED SCIENCES
OF
MIDDLE EAST TECHNICAL UNIVERSITY

BY

GÖKHAN ASLAN

IN PARTIAL FULLFILLMENT OF THE REQUIREMENTS
FOR
THE DEGREE OF MASTER OF SCIENCE
IN
MECHANICAL ENGINEERING

DECEMBER 2006

Approval of the Graduate School of Natural and Applied Sciences

_____

Prof. Dr. Canan Özgen
Director

I certify that this thesis satisfies all the requirements as a thesis for the degree of Master of Science.

_____

Prof. Dr. S. Kemal İder
Head of the Department

This is to certify that we have read this thesis and that in our opinion it is fully adequate, in scope and quality, as a thesis for the degree of Master of Science.

_____

Prof. Dr. Mehmet Çalışkan
Supervisor

Examining Committee Members

Prof. Dr. H. Nevzat Özgüven (METU, ME) _____

Prof. Dr. Mehmet Çalışkan (METU, ME) _____

Prof. Dr. Yalçın Tanık (METU, EE) _____

Assoc. Prof. Dr. Tolga Çiloğlu (METU, EE) _____

Asst. Prof. Dr. Yiğit Yazıcıoğlu (METU, ME) _____

I hereby declare that all information in this document has been obtained and presented in accordance with academic rules and ethical conduct. I also declare that, as required by these rules and conduct, I have fully cited and referenced all material and results that are not original to this work.

Name, Last Name: Gökhan Aslan

Signature :

ABSTRACT

CEPSTRAL DECONVOLUTION METHOD FOR MEASUREMENT OF ABSORPTION AND SCATTERING COEFFICIENTS OF MATERIALS

Aslan, Gökhan
M.Sc., Department of Mechanical Engineering
Supervisor: Prof. Dr. Mehmet Çalışkan

December 2006, 101 pages

Several methods are developed to measure absorption and scattering coefficients of materials. In this study, a new method based on cepstral deconvolution technique is proposed. A reverberation room method standardized recently by ISO (ISO 17497-1) is taken as the reference for measurements. Several measurements were conducted in a physically scaled reverberation room and results are evaluated according to these two methods, namely, the method given in the standard and cepstral deconvolution method. Two methods differ from each other in the estimation of specular parts of room impulse responses essential for determination of scattering coefficients. In the standard method, specular part is found by synchronous averaging of impulse responses. However, cepstral deconvolution method utilizes cepstral analysis to obtain the specular part instead of averaging. Results obtained by both of these two approaches are compared for five different test materials. Both of the methods gave almost same values for absorption coefficients. On the other hand, lower scattering coefficient values have been obtained for cepstral deconvolution with respect to the ISO method.

Keywords: Reverberation room, random-incidence absorption coefficient, random-incidence scattering coefficient, cepstral deconvolution, maximum-length sequence

ÖZ

MALZEMELERİN SES YUTMA VE SES SAÇMA KATSAYILARININ ÖLÇÜLMESİ İÇİN KEPSTRAL ARINDIRMA METODU

Aslan, Gökhan
Yüksek Lisans, Makina Mühendisliği Bölümü
Tez Yöneticisi: Prof. Dr. Mehmet Çalışkan

Aralık 2006, 101 sayfa

Malzemelerin ses yutma ve ses saçma katsayılarının ölçülmesi için bir çok metot geliştirilmiştir. Bu çalışmada, kepstral arındırma tekniğine dayalı yeni bir metot önerilmiştir. Ölçmeler için, ISO tarafından yakın bir zamanda standardlaştırılmış bir çınlama odası metodu (ISO 17497-1) referans olarak alınmıştır. Ölçeklendirilmiş bir çınlama odasında bir çok ölçme gerçekleştirilmiş ve sonuçlar bu iki metot yani standardda verilen metot ve kepstral arındırma metodu kullanılarak değerlendirilmiştir. İki metot, ses saçma katsayılarının tayini için temel olan dürtü yanıtlarının aynasal olarak yansıyan kısımlarının bulunmasında birbirlerinden ayrılmaktadır. Standard metotta, aynasal olarak yansıyan kısımlar, dürtü yanıtlarının eş zamanlı ortalamaları alınarak bulunur. Bununla birlikte, kepstral arındırma metodunda, aynasal olarak yansıyan kısmı elde etmek için ortalama almak yerine kepstral analiz yöntemini kullanır. Her iki yaklaşım kullanılarak beş farklı malzeme için elde edilen sonuçlar kıyaslanmıştır. Metotların ikisi de ses yutma katsayıları için hemen hemen aynı değerleri

vermiştir. Diğer yandan, kepstral arındırma metodunda, ISO metoduna göre daha düşük ses saçma katsayı değerleri elde edilmiştir.

Anahtar Kelimeler: Çınlama odası, rastgele geliş açılı ses yutma katsayısı, rastgele geliş açılı ses saçma katsayısı, kepstral arındırma, azami uzunluk serisi

to my parents

ACKNOWLEDGEMENTS

I wish to express my deepest gratitude and appreciation to my supervisor Prof. Dr. Mehmet Çalışkan who inspired, encouraged and supported me throughout of this study.

The author is grateful to Aslı Oflaz, Güneş Acar, Ulaş Barış Sarısoy, Soner Büyükatalay, Ozan Ürgüt, Ozan Keysan and Kürşad Büyükyıldırım for their invaluable friendship, support and contributions to this work.

The author would like to thank to İmdat Uğursu, Erdoğan Durmaz, Eyüp Turhan and Asım Uysal for their help in the construction of the experimental setup.

The author would like to express his gratefulness to Mahmut Özdemir, Rasih Sözen, Haluk Soran, Altan Özen and Ömer M. Tüfek for their help and support.

Finally, the greatest thanks go to my family for their endless support, patience and encouragement.

TABLE OF CONTENTS

LIST OF SYMBOLS AND ABBREVIATIONS

A_1	Equivalent sound absorption area of a room with a test specimen
A_2	Equivalent sound absorption area of an empty room
A_T	Equivalent sound absorption area of a material
c	The speed of sound
c_c	Complex cepstrum
c_p	Power cepstrum
c_r	Real cepstrum
$[C]$	Column matrix
d	Diameter of the base plate
E_{abs}	Energy absorbed on a surface
E_i	Energy of a incident sound wave
$E_{r,scat}$	Energy scattered from a surface
$E_{r,spec}$	Energy reflected specularly from a surface
$E_{r.total}$	Energy reflected from a surface
$E(t)$	Energy decay curve as a function of time
f	Frequency
$f_{\max}$	Highest frequency component
f_N	Nyquist frequency
f_{rO}	Relaxation frequency of oxygen
f_{rN}	Relaxation frequency of nitrogen
f_s	Sampling frequency
f_s	Schroeder frequency

$F\{\ \}$	Fourier transform
$F^{-1}\{\ \}$	Inverse Fourier transform
FHT	Fast Hadamard transform
h	Structural depth of a sample
h	Molar concentration of water vapor
h_r	Mean relative humidity of the air inside the room
$h(t)$	Impulse response function
$[h]$	Impulse response in matrix form
H	Hadamard matrix
$I_{\max}$	Longest straight line within the room
k	Sample number
k	Wave number
l	Length of a maximum length sequence
l	Linear filter
L_x, L_y, L_z	Room dimensions in x-, y- and z- direction, respectively
m	The energy attenuation coefficient of air
m	Arbitrary number
MLS	Maximum-length sequence
n	Arbitrary number
n	Order of a maximum length sequence
n_x, n_y, n_z	Mode numbers in x-, y- and z-direction, respectively
N	Physical scale ratio
p	Sound pressure
p_a	Ambient atmospheric pressure
p_r	Reference atmospheric pressure of 101.325 kPa
p_{sat}	Saturation vapor pressure
$p(\tau)$	Impulse response

$[R]$	Row matrix
s	Random-incidence scattering coefficient
s_{base}	Scattering coefficient of the base plate
$s(t)$	Input signal of a system
$s'(t)$	Output signal of a system
S	Area of the specimen
S	Power spectrum
$[S]$	Input signal in matrix form
$[S']$	Output signal in matrix form
t	Time
T	Air temperature
T	Reverberation time
T_0	Period of the input signal
T_0	Reference air temperature
T_1	Reverberation time without sample and turntable is not rotating
T_2	Reverberation time with sample and turntable is not rotating
T_3	Reverberation time without sample and turntable is rotating
T_4	Reverberation time with sample and turntable is rotating
T_{01}	Triple-point isotherm temperature of 273.16 K
T_{10}	Reverberation time evaluated between -5 dB and -15 dB
T_{15}	Reverberation time evaluated between -5 dB and -20 dB
T_{20}	Reverberation time evaluated between -5 dB and -25 dB
T_{30}	Reverberation time evaluated between -5 dB and -35 dB
V	Volume of the room
$x(t)$	Arbitrary function
x, y, z	Cartesian coordinates

α	Sound pressure attenuation coefficient
α_s	Random-incidence absorption coefficient
α_{spec}	Random-incidence specular absorption coefficient
$\overline{\alpha}_d$	Average diffuse-field surface absorption coefficient
$\delta(t)$	The Dirac function
τ	Delay time
ω	Angular frequency
Φ	Correlation function
$*$	Convolution operator

CHAPTER 1

INTRODUCTION

Absorption and scattering properties of the materials used on the interior of public spaces such as auditoria, concert halls, airport terminals or work spaces, industrial facilities, workshops alike play an important role in the acoustical quality of these spaces. These properties are very crucial especially in the acoustical design of such places which characterize audibility and acoustical comfort in these spaces. As stated in ISO 17497-1 “Together with the absorption coefficient, scattering coefficient will be useful in room acoustic calculations, simulations and prediction models. For some time it has been known that modeling of the scattering from surfaces is very important for obtaining reliable predictions of room acoustics” [1].

1.1 Absorption and Scattering

When sound waves strike the surface of a material, incident sound energy is separated into four parts; energy absorbed by the surface, reflected back from the surface, transmitted through the material and transmitted into the material (see Figure 1.1).

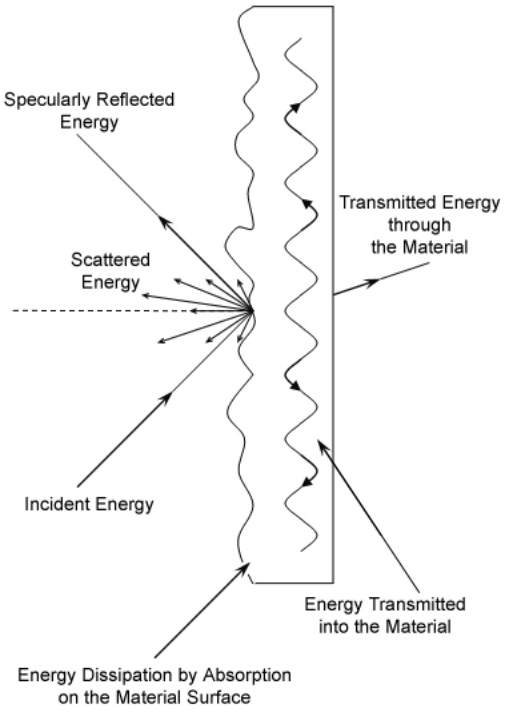

Figure 1.1 – Energy manipulation mechanisms result from interaction between incident sound wave and surface of a material

Absorption of a surface is directly related to pattern of the surface i.e. absorption increases with roughness as well as material properties such as its porosity, fiber diameter, structure factor and flow resistivity [2]. Another mechanism influenced from the surface pattern is reflection of the incident sound. As shown in Figure 1.1, energy is reflected in two ways; specular reflection and scattering. When the angle of incidence of a sound wave is equal to the angle of reflection with respect to the surface normal this kind of reflection is called as specular. The rest of the reflected energy can be considered as scattered.

1.2 Absorption and Scattering Coefficients

Sound absorption coefficient of a material is expressed as the ratio of the equivalent sound absorption area of the material sample to the area of the material sample being tested [3]. The equivalent sound absorption area of a material sample A_T is found by subtracting the equivalent sound absorption of an empty reverberation room (A_2) from the equivalent sound absorption of the room with the test specimen (A_1). The equivalent sound absorption of a room mentioned above stands for the "hypothetical area of a totally absorbing surface without diffraction effects which, if it were the only absorbing element in the room, would give the reverberation time as the room under consideration" [3].

For a rigid material stuck in front of a hard wall, energy transmission through and into the material can be ignored (see Figure 1.2). Then it could be assumed, the energy of the incident sound wave E_i is equal to the sum of the energy absorbed on the material surface E_{abs} and the energy reflected from the surface $E_{r.total}$ and the absorption and scattering coefficients defined in ISO 17497-1 could be written as follows [1]:

Random-incidence scattering coefficient (s):

$$s = 1 - \frac{E_{r,spec}}{E_{r,total}} = \frac{E_{r,scat}}{E_{r,total}} \tag{1.1}$$

Random-incidence absorption coefficient (α_s):

$$\alpha_s = 1 - \frac{E_{r,total}}{E_i} = \frac{E_{abs}}{E_i} \tag{1.2}$$

Random-incidence specular absorption coefficient (α_{spec}):

$$\alpha_{spec} = 1 - \frac{E_{r,spec}}{E_i} = \frac{E_{r,scat} + E_{abs}}{E_i} \tag{1.3}$$

Here $E_{r,spec}$, $E_{r,scat}$ and $E_{r,total}$ denote reflected acoustical energies from a surface specularly, scattered and total respectively. E_{abs} is the energy absorbed on a surface and E_i denotes the incident acoustical energy to a surface.

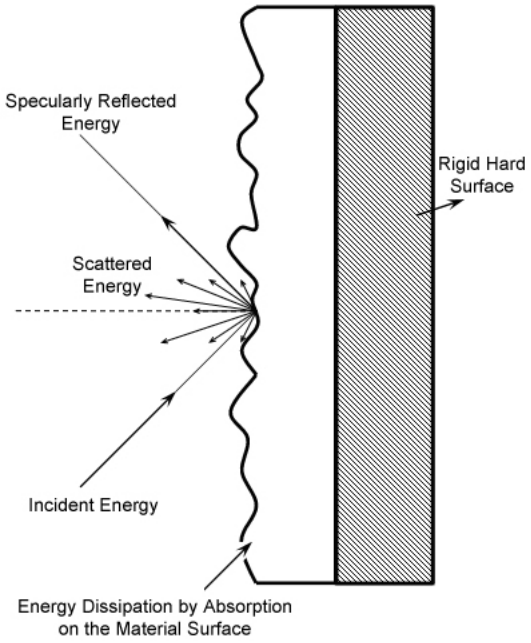

Figure 1.2 – Change in energy manipulation mechanisms as a result of sticking the material into a hard surface

1.3 Motivation and Objective

In this study, a new method is to be developed to measure random-incidence absorption and scattering coefficients of materials in a reverberation room. For this purpose, a physically scaled reverberation room is to be designed and constructed. Measurements for five different materials are to be conducted and measurement results are evaluated for two different method; standard ISO method and cepstral deconvolution method. These methods are compared in terms of results obtained for absorption and scattering coefficients.

Both of the methods use same data acquired in reverberation room. However, the new method differs from the ISO method in decomposition of impulse responses in terms of their specular and scattered parts. In the new method, specular parts are separated from the rest of the impulse responses by employing cepstral analysis instead of time averaging of impulse responses. By this way, it is expected specular parts could be obtained more accurately i.e. immune to noise caused by scattered parts of impulse responses.

In experiments, a broadband excitation signal (maximum-length sequence) is used. And estimated absorption and scattering coefficients are presented in one-third-octave bands with center frequencies of 100 Hz to 2000 Hz.

1.4 Organization

In this thesis, all of the goals are accomplished in six chapters. In Chapter 2, previous studies related to the subject of this thesis i.e. measurement of reverberation time and determination of absorption and scattering coefficients are reviewed. Third chapter describes theoretical background and the procedure followed in the reverberation room measurements. In addition, corresponding calculations for absorption scattering coefficients are given in this chapter. Fourth chapter depicts cepstral analysis in terms of definition and formulation of real,

power and complex cepstrum and cepstral deconvolution. Moreover, all steps of application procedure of deconvolution followed in this study are specified. Chapter 5 includes specifications of measurement setup and test materials. Also, experimental procedures for both methods, results in graphical form and comments about them are presented in this chapter. Finally, in the last chapter, a brief summary of this study, conclusions about the results obtained and comparison of the methods and furthermore, recommendations for possible future works are given.

CHAPTER 2

LITERATURE SURVEY

2.1 Introduction

Acoustical measurements can be classified in two groups with respect to where they are carried out; free-field measurements and measurements performed in enclosures. Measurement of reverberation time needs to be performed in an enclosure. In fact, reverberation time is one of the most frequently used properties in evaluation of acoustical quality of enclosures. On the other hand, absorption and scattering coefficients of materials can be estimated from different type of measurement methods performed both in free-field conditions and inside an enclosure such as impedance tube or reverberation room.

Reverberation rooms are conventionally used to measure acoustical properties of materials regarding their sound absorption behavior, acoustical power of sound sources and transmission of sound in between building elements [2]. They are designed in order to provide an approximate diffuse sound field. Hence, determination of acoustical properties via prediction of sound fields developed in a room can be achieved using diffuse-field theory which is starting point for “the best known theoretical models for predicting room sound fields” [2].

Diffuse-field can be described by two fundamental characteristics; intensity of energy incident to any point in the room does not vary with respect to directivity and the value of intensity does not change from position to position inside the room.

Among others, Sabine's diffuse-field model is the most applicable model in case of determination of sound absorption coefficient of materials in a reverberation room [2]. For rooms having sufficiently low average absorption coefficient for its surfaces i.e. less than 0.25, sound decay in this enclosure can be described by the formula below for a point source.

$$T_{60} = \frac{55.3V}{c\left[4mV - S.\overline{\alpha}_d\right]} \tag{2.1}$$

Here, T_{60} stands for reverberation time in seconds, S and V denotes total surface area in m^2 and volume in m^3 of the room, respectively. c is the speed of sound in air in m/s. m energy attenuation coefficient of air in Np/m and $\overline{\alpha}_d$ specifies average diffuse-field surface absorption coefficient.

2.2 Previous Studies

In 1965, Schroeder [4] described a new method to measure reverberation times in enclosures. According to this method, an enclosure is excited by a random noise such as pistol shot. Then, reverberation time is determined from corresponding decay curve obtained from integration of squared room impulse responses in reverse direction in time domain i.e. Schroeder's backward integration. Therefore, need for repeating measurements many times and ensemble averaging of decay curves to eliminate unwanted random fluctuations existed in resulted curves is no longer required. Measurements could be carried out with much better accuracy in a single measurement by using this method.

In reverberation time measurements utilizing integrated impulse response method, an excitation signal having flat spectrum should be employed. Conventional impulse sources like pistol shots or electric sparks may not satisfy that flat spectrum requirement and also loudspeakers used could not be driven

with such an instantaneous signal providing necessary signal-to-noise ratio [5]. In 1979, Schroeder [5] proposed to use of maximum-length sequences in measurement of impulse responses of linear systems. By this way, requirement for flat spectrum is fulfilled and a considerable increase in signal-to-noise ratio is achieved.

In 1990, Chu [6] presented a detailed application procedure of maximum-length sequences in determination of impulse response and reverberation decay. In his study, advantages of using a periodic pseudorandom sequence, i.e. maximum-length sequences, in noisy environments demonstrated together with experimental results.

Maximum-length sequences were also employed in measurement of scattering on hard wall surfaces with highly diffuse behavior [7]. As stated by Schroeder, flat power spectra of these type signals make them ideal for use of design purposes of such surfaces.

In 1995, Vorländer and Mommertz [8] presented a new measurement method for determination of random-incidence scattering coefficients and this method was published in 2000 for free field and reverberation room applications. Their method was based on the separation of highly coherent specular part of the reflection from the total reflection by synchronous averaging of sufficient number of impulse responses obtained for different orientations of the sample surface. After this averaging procedure it could be possible to evaluate the random-incidence scattering coefficient from the remaining part of the impulse response because averaging cancels out statistically independent scattered parts of the reflection. In 2004 this method was standardized by ISO for reverberation room measurements with standard number of ISO 17497-1 [1]. This method was used in a development study of some scattering surfaces for concert halls by Jeon *et al* [9]. They employed the method in a scaled reverberation room for the evaluation

of the effects of the size, and the structural density of different geometries located over a surface on the scattering properties of the surface.

In addition to measurement methods disregarding directional distribution of sound reflection, a method using directivity of reflected sound waves in determination of scattering coefficient was introduced by Mommertz [10].

An additional quantity to evaluate acoustical properties of surfaces is known as diffusion coefficient. It is used in evaluation of scattering uniformity of a surface for incident sound waves. A free-field measurement method has been proposed by Audio Engineering Society to evaluate both directional and random-incidence diffusion coefficients of surfaces [11].

Another free-field measurement method for absorption and scattering coefficients, namely, wave field synthesis method has been presented by Farina [12]. In this method, receiver (microphone) is moved on a straight line and specimen being tested is kept steady. Results obtained for this method and the method stated by Mommertz and Vorländer for scattering coefficient and AES method for diffusion coefficient were compared [12, 13].

CHAPTER 3

REVERBERATION ROOM MEASUREMENTS

3.1 Introduction

The theory behind the measurement in a reverberation room is based on the energy balance established between the energy income in the form of sound into the enclosed space (reverberation room) through a sound source and the energy converted into the forms other than sound basically. The former increases the sound pressure level inside the enclosure and the latter affects the internal sound pressure level reversely. When this enclosed space is excited by operating a sound source, a reverberant sound field is developed inside the space and for a constant energy input steady state energy condition is reached by means of the sound absorption mechanisms due to the boundary surfaces, the gas filling the space and other objects within the space [3]. After turning off the sound source, the sound energy within this enclosed space decreases exponentially due to this energy dissipation phenomena. In this region where the sound energy decreases, the room impulse response is evaluated in time domain. Then, the decay curve of the sound pressure level is obtained from the impulse response between a particular pair of sound source and receiver. This is the "most fundamental physical descriptor in room acoustics" as Schroeder's backward integration depicts [6]. This curve gives us the reverberation time which is the time required for the sound pressure level decreases by 60 dB after the sound source is turned off in seconds for that measurement. This decrease corresponds to a drop to one millionth of original acoustic pressure on linear scale.

The method described in ISO 17497-1 is based on the assumption that scattered components of impulse responses for different positions of a material are statistically independent from each other [1, 8]. According to this assumption specular part of the energy reflected form the surface of a material can be extracted from the impulse response by using "synchronized averaging" of impulse responses obtained during a period of a measurement for different positions of the material [1]. This averaging procedure results in the scattered components of the impulse responses cancelled out each other and the remaining part is just consisted of "highly correlated" specular components of the reflection [1]. In practice, a test sample is placed on a turntable in a reverberation room and impulse responses are collected while the sample is rotated during the measurement. Then, the averaged impulse response is used in further calculations. If the sample shows a perfect specular reflection characteristic and also the sample is circular in shape the results of measurements for which turntable is rotating and not rotating shows an excellent correlation [8]. Deviations from this perfect correlation are directly related to the diffuse reflections (i.e. scattering) which are exhibited by the sample being tested [8].

As shown in Figure 3.1 initial parts of the impulse responses are much more correlated than the later parts. This is because of the phase differences resulting from the change in orientation [1]. According to Vorländer and Mommertz this is reasonable since the primary part of each impulse response represents the sound waves which have traveled the distance between the sound source and microphone in a shorter time without being influenced from scattering [8].

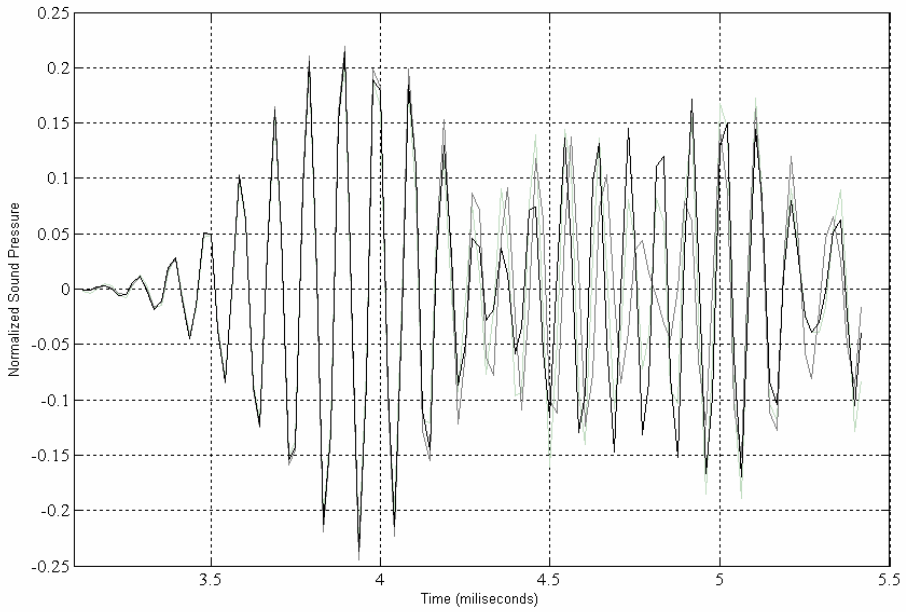

Figure 3.1 – Impulse responses for three different orientation of the specimen

3.2 The Reverberation Room

Tracing the propagation of the sound in a enclosed space is very difficult task and needs more sophisticated equipment in terms of the determination of angles for incidence or reflection of sound beams. Because of that, it is much common to use an appropriate average value rather than values with respect to their directivity pattern for absorption and scattering coefficients. In most of the acoustical applications usually these coefficients are presented and employed in the form of an average value independent of any specific angular information, i.e. random-incidence values [3, 8]. As pointed out in ISO 354, if the sound intensity within an enclosed space is uniform, the sound field inside this enclosure is called as diffuse and the sound coming to any surface in that space is "said to be at random-incidence" [3]. Therefore the sound field in the reverberation room

should be as diffuse as possible during the random-incidence absorption and scattering coefficient measurements.

There exist two types of reverberation rooms in manner of scale i.e. full scale and physical scale. The latter is the same as the first except all of its linear dimensions are scaled by a ratio $1:N$ which is called as "physical scale ratio" [1]. While all the dimensions of the reverberation room are reduced according to this ratio, frequencies of interest are increased at the same rate and *vice versa*. Because, in scaled reverberation room measurements wavelength of the sound used should be scaled too as long as the speed of sound remains same as in the full scale [1]. Therefore, a physical scale model of a material and a reverberation room can be used to represent their full scale models. For instance, result of a measurement done for any material scaled with a ratio of $1:10$ at the frequency of 10 kHz in a reverberation room scaled with the same ratio could be used to represent corresponding measurement result for the full scale model of the material obtained at 1 kHz in a full scale reverberation room.

3.3 Test Signals

The definition of the impulse response states that an impulsive source is operated at a particular location in a room and this impulse results in changes in the properties of medium (i.e. air) such as in sound pressure level at another location in the room (receiver position) and this change with respect to time is called as impulse response [3, 14]. As stated by Kuttruff the impulse response of a linear transmission system involves all of the properties of this system, an impulse response of a room accepted as an "acoustical transmission system" can provide information about all of the changes (including the one about the sound pressure level) that a sound signal being subjected all along the path it traveled between the source and the receiver [14].

The Dirac function $\delta(t)$ is defined as follows:

$$\begin{aligned} &\delta(t) = \infty \qquad for\ t = 0 \\ &\delta(t) = 0 \qquad for\ t \neq 0 \end{aligned} \tag{3.1}$$

This means, the Dirac function is represented at a single point and with amplitude of infinity in time domain. On the other hand, the Fourier transform of the Dirac function which gives its spectral energy distribution in frequency domain exhibits a uniform characteristic (i.e. flat spectrum) for all frequencies.

$$\begin{aligned} &\int_{-\infty}^{\infty} \delta(t)\, dt = 1 \\ &F\{\delta(t)\} = \int_{-\infty}^{\infty} \delta(t)\, e^{-2\pi i f t} dt = 1 \end{aligned} \tag{3.2}$$

By using the property of the Dirac function, any signal as a function of time $s(t)$ can be represented as follows [14]:

$$s(t) = \int_{-\infty}^{\infty} s(\tau)\, \delta(t-\tau)\, d\tau \tag{3.3}$$

This equation demonstrates the relationship between the output and input with respect to the impulse response of a linear system (i.e. anything changes the input of the system changes the output by the same factor).This can be used also to represent any linear transmission system in terms of input $s(t)$, impulse response $h(t)$ instead of Dirac function $\delta(t)$ and output $s'(t)$ of the system.

$$s'(t) = \int_{-\infty}^{\infty} s(\tau)\, h(t-\tau)\, d\tau \tag{3.4}$$

This is called as the convolution operation between the functions *s(t)* and *h(t)* [14]:

$$s'(t) = s(t) * h(t) = h(t) * s(t) \tag{3.5}$$

If the input *s(t)* and the output *s'(t)* of a linear time-invariant system are known it is possible to obtain the impulse response of this system *h(t)* by applying deconvolution to the convolved signal as mentioned above. Deconvolution is done by estimation of the cross-correlation between the input and output signals as shown below [14]:

$$\begin{aligned}
\Phi_{ss'}(\tau) &= \lim_{T_0 \to \infty} \frac{1}{T_0} \int_{-T_0/2}^{+T_0/2} s(t)\, s'(t+\tau)\, dt \\
&= \lim_{T_0 \to \infty} \frac{1}{T_0} \int_{-T_0/2}^{+T_0/2} s(t)\, dt \int_{-\infty}^{+\infty} h(t')\, s(t+\tau-t')\, dt' \\
&= \int_{-\infty}^{+\infty} h(t') \left[\lim_{T_0 \to \infty} \frac{1}{T_0} \int_{-T_0/2}^{+T_0/2} s(t)\, s(t+\tau-t')\, dt \right] dt'
\end{aligned} \tag{3.6}$$

here T_0 is the duration of the corresponding input signal.

Because of the term in brackets in equation (3.6) is represents the auto-correlation function of the input signal, the cross-correlation function can be expressed as

$$\Phi_{ss'}(\tau) = \int h(t')\, \Phi_{ss}(\tau - t')\, dt' \tag{3.7}$$

In consequence, the expression above means, the cross-correlation function of the input and the output of a linear system gives the impulse response of this system if the auto-correlation of the input signal is exactly or at least approximately a delta function like as the Dirac function in equation (3.3) [14]. Moreover the

cross-correlation procedure provides almost a noise immune measurement even under conditions with high background noise [6].

It is impossible to generate an exact Dirac impulse and this deconvolution procedure works well especially for broadband signals with a flat spectrum. Therefore, a broadband excitation signal which results in sound pressure levels over all of the frequency bands of interest nearly equal (i.e. flat spectrum) like a Dirac impulse (such as white noise, maximum-length sequences or linear sine sweeps) could be employed to measure the response of the room [14]. Then, this response is used with a transformation technique specific to the excitation signal employed to obtain the impulse response. Moreover, as the method requires a consistent averaging of room impulse responses, the test signal should be kept unchanged from measurement to measurement as well [1, 3].

3.3 Maximum Length Sequence and Fast Hadamard Transform

The measurement technique which uses a periodic pseudo-random noise MLS (maximum-length sequence or *m*-sequence) as the source signal is based on a cross-correlation method to determine the impulse response. In auto-correlation functions of random noises, amplitude is concentrated at $\tau = 0$ [14]. Likewise, in the auto-correlation function of any MLS signal, amplitude is concentrated at the first sample with a value of length of the MLS signal and the rest of the function composed of minus ones (Figure 3.2). Hence, it is called as a random noise. Because of the technique employs a large series of deterministic pulses with a desired length, a very high signal-to-noise ratio could be obtained [6].

A maximum-length sequence is made up of a binary sequence whose elements are equal in amplitude and have a sign pattern differs sequence to sequence according to tap positions selected (see Appendix B). It is generated by a "n-step shift register" with an arrangement which feeds the input with outputs of the exclusive-OR, XOR, (or modulo-2 arithmetic) operation. Where n designates the

order of the corresponding sequence and a period of an MLS of order n consisted of $l = 2^n - 1$ elements.

Auto-correlation of a continuous signal $s(t)$ is described as below [14]

$$\Phi(\tau) = \lim_{T_0 \to \infty} \frac{1}{T_0} \int_{-T_0/2}^{+T_0/2} s(t)\, s(t+\tau)\, dt \tag{3.8}$$

For a maximum-length sequence s_k , $k = 1, 2, ..., l$, as a periodic (i.e. $s_{k+l} = s_k$) but discrete signal its auto-correlation function can be expressed as

$$\Phi_{ss}(m) = \sum_{k=1}^{l} s_k \; s_{k+m} \tag{3.9}$$

As shown in Figure (3.2) the auto-correlation function has values

$$\Phi_{ss}(m) = \begin{cases} l & \text{, for } m = 1 + n \cdot l \text{ where } n = 0, 1, 2, ... \\ -1 & \text{, for other values of } m \end{cases}$$

which approves the randomness of the MLS signal as mentioned before.

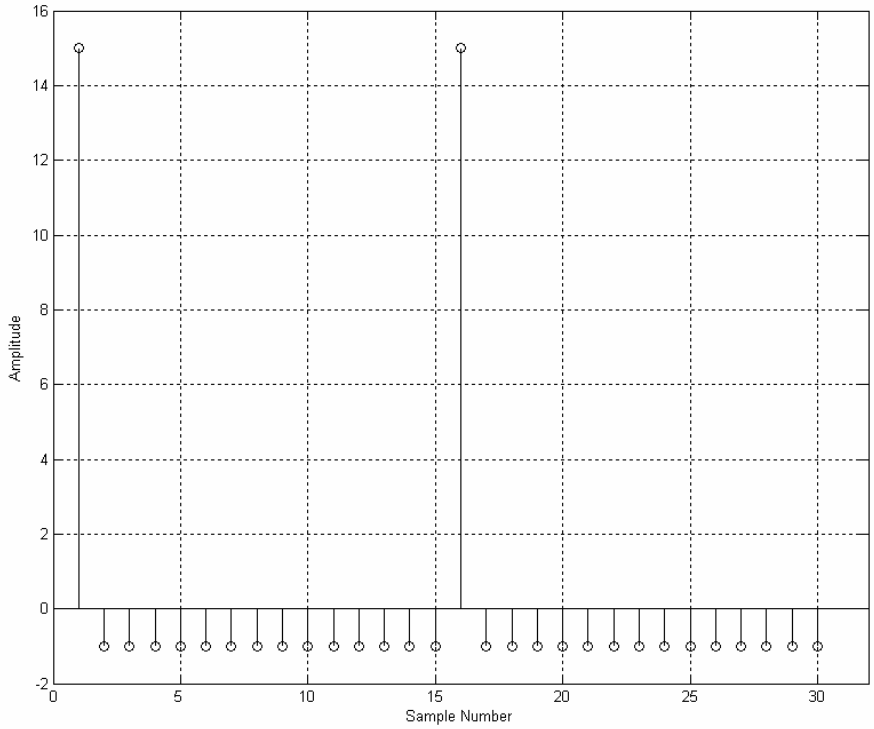

Figure 3.2 – Auto-correlation function of two successive MLS signals of order 4

Sampling rates of input signals which are generated from a maximum-length sequence and output signals should be same. In other words, the time interval Δt existing between the two consecutive pulses of an MLS signal must be equal to reciprocal of the sampling frequency f_s of the output signal such that

$$\Delta t = \frac{1}{f_s} \tag{3.10}$$

In addition to that the sampling frequency should be at least two times the highest frequency component $f_{\max}$ of interest in the measurements so called "Nyquist frequency" f_N in accordance with Nyquist's sampling theorem

$$f_{\max} = \frac{1}{2} f_N < \frac{1}{2} f_s \tag{3.11}$$

Following the emission of MLS as an input signal the output signal s'_k which is the convolution between the input signal and the corresponding impulse response h_{k-i} can be expressed in discrete form as follows [14]

$$s'_k = \sum_{i=1}^{l} s_i \, h_{k-i} \tag{3.12}$$

In matrix form

$$[S'] = [S] \cdot [h] \tag{3.13}$$

or

$$\begin{bmatrix} s'_1 \\ s'_2 \\ s'_3 \\ \vdots \\ s'_l \end{bmatrix} = \underbrace{\begin{bmatrix} s_1 & s_2 & s_3 & \cdots & s_l \\ s_2 & s_3 & s_4 & \cdots & s_1 \\ s_3 & s_4 & s_5 & \cdots & s_2 \\ \vdots & \vdots & \vdots & \vdots & \vdots \\ s_l & s_1 & s_2 & \cdots & s_{l-1} \end{bmatrix}}_{l \text{ elements}} \begin{bmatrix} h_l \\ h_{l-1} \\ h_{l-2} \\ \vdots \\ h_1 \end{bmatrix} \tag{3.14}$$

At this point there are two particular ways to solve the matrix above in order to determine the impulse response of the system:

A) Direct solution with matrix multiplication

First of all input and impulse response matrices in equation (3.14), [S] and [h] respectively, are changed as shown below

$$[S]_{\text{modified}} = \underbrace{\begin{bmatrix} 1 & 1 & 1 & \cdots & 1 \\ 1 & s_1 & s_2 & \cdots & s_l \\ 1 & s_2 & s_3 & \cdots & s_1 \\ \vdots & \vdots & \vdots & \vdots & \vdots \\ 1 & s_l & s_1 & \cdots & s_{l-1} \end{bmatrix}}_{l+1 \text{ elements}}$$

$$[h]_{\text{modified}} = \begin{bmatrix} 0 \\ h_l \\ h_{l-1} \\ \vdots \\ h_1 \end{bmatrix}$$

Then, the corresponding output matrix becomes

$$[S']_{\text{modified}} = \begin{bmatrix} \sum_{i=1}^{l} h_i \\ s_1' \\ s_2' \\ \vdots \\ s_l' \end{bmatrix}$$

Equation (3.13) is rearranged for modified matrices and both sides of the equation is multiplied by the modified S matrix

$$[S]_{\text{modified}} \cdot [S']_{\text{modified}} = [S]_{\text{modified}} \cdot [S]_{\text{modified}} \cdot [h]_{\text{modified}} \tag{3.15}$$

Due to its specific property, multiplication of modified S matrix with itself gives a unit matrix such that

$$[S]_{\text{modifed}} \cdot [S]_{\text{modifed}} = (l+1)\begin{bmatrix} 1 & 0 & \cdots & 0 \\ 0 & 1 & \cdots & 0 \\ \vdots & \vdots & \vdots & \vdots \\ 0 & 0 & \cdots & 1 \end{bmatrix} \tag{3.16}$$

Then equation (3.15) becomes

$$[S]_{\text{modified}} \cdot [S']_{\text{modified}} = (l+1)[h]_{\text{modified}} \tag{3.17}$$

Impulse response h_k can be obtained removing the very first element after multiplication of the modified MLS matrix (consisted of left shifted MLS elements) and the modified output matrix divided by the length of the MLS signal as shown below

$$[h]_{\text{modified}} = \frac{1}{l+1}[S]_{\text{modified}} \cdot [S']_{\text{modified}} \tag{3.18}$$

B) Fast Hadamard transform solution

The fast Hadamard transform is used to perform the matrix multiplication in equation (3.18) in a very fast and efficient way. This procedure consists of the transformation of an MLS matrix of dimensions $(l)\times(l)$ to a Hadamard matrix of dimensions $(l+1)\times(l+1)$ by some modifications and usage of the information

obtained throughout this transformation process in re-modification of the resultant matrix obtained.

The basic structure of a $(2^n)\times(2^n)$ Hadamard matrix of order n can be described as [14]

$$H_n = \begin{bmatrix} H_{n-1} & H_{n-1} \\ H_{n-1} & -H_{n-1} \end{bmatrix} \text{ where } H_0 = 1$$

The transformation procedure follows the one described by Chu [6].

First of all, the elements of the MLS matrix of order n are replaced by 0 and 1 instead of 1 and -1. Then, the resultant matrix "factored" into a column matrix [*C*] and a row matrix [*R*] [6]. [*C*] matrix (of dimensions $n \times l$) is included the first n rows of the matrix [*S*] and [*R*] matrix (of dimensions $l \times n$) is composed of the n columns of [*S*] such that their first n rows construct an $n \times n$ unit matrix. Then, the columns of [*C*] and the rows of [*R*] are "tagged" by converting their elements from binary to decimal. In this process it should be ensured that the most significant digit is located at the first row and at the first column for columns and rows, respectively.

Next, by using the tags obtained for [*C*], the columns of the [*S*] are reordered. After that the same procedure is done for the rows of the changed matrix [*S*]' according to the tags of [*R*] so a new matrix [*S*]"is generated.

Then, the new matrix [*S*]" is modified again by adding a row and column of ones and it becomes an Hadamard matrix of order n.

$$[S]''' = \underbrace{\begin{bmatrix} 1 & 1 & 1 & \cdots & 1 \\ 1 & [S]''_{11} & [S]''_{12} & \cdots & [S]''_{1l} \\ 1 & [S]''_{21} & [S]''_{22} & \cdots & [S]''_{2l} \\ \vdots & \vdots & \vdots & \vdots & \vdots \\ 1 & [S]''_{l1} & [S]''_{l2} & \cdots & [S]''_{ll} \end{bmatrix}}_{l+1 \text{ elements}} \tag{3.19}$$

Meanwhile the elements of the output matrix [S'] are rearranged by using the tags for [C] and a zero is added this matrix. Therefore the result is a $(l+1)$ by 1 matrix[S']".

Finally, matrix multiplication is performed between the Hadamard matrix H (or equivalently [S]"') and rearranged output matrix [S']" using the butterfly algorithm.

$$[h]'' = [S]''' \cdot [S']'' \tag{3.20}$$

The result gives a modified version of the impulse response[h]". In order to obtain the actual impulse response [h], the first element of [h]" is removed and the elements of this new matrix [h]' are reordered according to tags of [R].

The major point of the fast Hadamard transform is that, because the Hadamard matrix has a special matrix structure, it enables to perform the matrix multiplication mentioned above with the use of a very efficient "butterfly" algorithm. While the matrix multiplication in the classical way as described in solution A requires $(l) \times (l-1)$ number of arithmetical operation, only $(l+1) \times \left[\log_2(l+1)\right]$ number of operations are required to achieve the matrix multiplication according to the way described in solution B [6].

A simple example for generation of a maximum-length sequence (MLS) and application of the fast Hadamard transform (FHT) is given in Appendix B.

3.4 Measurement Procedure

The measurement procedure below follows the requirements of ISO 354 and ISO 17497-1 [1, 3]. First of all the reverberation times T_1 and T_2 "without and with test sample", respectively are obtained from the measured impulse responses while the turntable is not rotating. Then, this is repeated for a rotating turntable to get reverberation time T_3 without the test sample and reverberation time T_4 with the test sample. During the measurements, while the turntable is operating, excitation signals should be propagated in equal time steps for a measurement period. This means the total time required for n number of periodic test signals to be radiated should be equal to the time elapsed in one revolution of the turntable at constant speed. The test signal should be same for all measurements during the tests. This is required to get a time invariant impulse response obtained from the averaged n measurements. Averaging could be performed before or after calculating the impulse responses. The number of impulse responses to be averaged should be within the range 60 to 120 [1]. This number is also equal to the number of excitation signals radiated during a measurement period.

To obtain the decay curve of the sound pressure level from the averaged impulse responses "integrated impulse response method" is employed as stated in ISO 354 [3]. In this procedure Schroeder's backward integration technique is applied to the impulse response. The result is a linearly decreasing curve for T_1, T_2 and T_3 measurements and "two superimposed decay curves" for T_4 measurements where the reverberation time should be evaluated from the first one [1]. It should be noted that in this part of the method it is assumed "there is a linear relationship between the sound pressure level and time and that the background noise level is sufficiently low" [3].

In the determination of the reverberation times from decay curves the upper limit of the evaluation range should be 5 dB below the highest sound pressure level of the impulse response and the lower limit should be 10 dB above the background noise level [3]. In order to obtain the reverberation time a least squares fit line algorithm is performed on the evaluation range and the resultant fit line is used to determine the corresponding reverberation time [3].

Measurement procedure should be repeated for at least six times. This is combination of at least two different sound source positions and at least three different microphone positions [1]. Then, evaluated reverberation times for the same sample and turntable configuration (e.g. six T_2 for different positions) are averaged arithmetically in spatial manner and this averaging is performed for each four different reverberation times to obtain their final value before further calculations [1].

Another argument is the frequency dependency of the absorption and scattering coefficients and impulse responses. The absorption and scattering coefficients of the materials are presented in frequency bands, because, response of a material differs for wavelength and therefore frequency components of incident sound wave. In measurements, employing a broadband test signal could be very advantageous instead of band limited signals. Since, this enables to measure most of the acoustical properties for different frequency bands in a single measurement. Then, impulse responses are filtered in specific frequency bands before or after the averaging. For this type of measurements, it is recommended to use one-third octave bands in the range of 100 Hz to 5000 Hz of center frequencies [3].

3.5 Schroeder's Backward Integration

According to this technique the decay curve is obtained by integrating the squared impulse response in reverse direction along the time axis. Ideally, when no background noise exists, integration starts from the end of the squared impulse response (corresponds to infinity in theory) and continues back to its beginning. The resulting energy decay curve in time domain is given as follows [3]:

$$E(t) = \int_0^{\infty} p^2(\tau)d\tau - \int_0^{t} p^2(\tau)d\tau = \int_t^{\infty} p^2(\tau)d\tau = \int_{\infty}^{t} p^2(\tau)d(-\tau) \tag{3.21}$$

where $E(t)$ denotes decay curve as a function of time results from integration, $p(\tau)$ and t stands for impulse response and corresponding time for the beginning of the impulse response, respectively.

Level of the background noise existing during the tests is an important factor that influences accuracy of the measurements. Therefore, limits of the integration should be chosen carefully. If the background noise could be determined, the integration should be started from the intersection point t_1 where the horizontal line of the background noise level and the linear slope of the decaying curve relevant to the estimation of the reverberation time cross each other as described in ISO 354 [3]. Then the decay curve could be expressed as:

$$E(t) = \int_{t_1}^{t} p^2(\tau)d(-\tau) + \int_{\infty}^{t_1} p^2(\tau)d(-\tau) \tag{3.22}$$

where the second term on the right hand side of the equation represents an optional correction [3]. This term could be estimated due to the assumption that the exponential energy decay continues after the time t_1 with the same rate of squared impulse response between t_1 and t_0 which is the time where the sound

pressure level is 10 dB higher than the one at t_1 [3]. Ignoring this correction may cause an underestimated reverberation time [3].

3.6 Normal Modes of the Room and Schroeder Frequency

As depicted by Kuttruff [14], in order to represent the sound field in an enclosure Helmholtz equation can be used as

$$\nabla^2 p + k^2 p = 0$$
or
$$\frac{\partial^2 p}{\partial x^2} + \frac{\partial^2 p}{\partial y^2} + \frac{\partial^2 p}{\partial z^2} + k^2 p = 0 \tag{3.23}$$

with boundary conditions assuming enclosure is surrounded by rigid walls, i.e. pressure change on boundaries along the wall normal is zero

$$\begin{aligned} &\frac{dp}{dx} = 0 \qquad for\ x = 0 \text{ and } x = L_x \\ &\frac{dp}{dy} = 0 \qquad for\ y = 0 \text{ and } y = L_y \\ &\frac{dp}{dz} = 0 \qquad for\ z = 0 \text{ and } z = L_z \end{aligned} \tag{3.24}$$

The equation above gives non-zero solutions for some specific k values (wave numbers) in the form of $p(x, y, z)$. These solutions denote standing waves in the enclosure and also known as normal modes of the room [14].

For a rectangular room with rigid perfectly reflecting walls, frequencies of the normal modes of the room can be found according to the formula

$$f_{n_x n_y n_z} = \frac{c}{2\pi} k_{n_x n_y n_z} \tag{3.25}$$

where c is the speed of sound (m/s) and $k_{n_x n_y n_z}$ is the wave number of the propagating sound such that

$$k_{n_x n_y n_z} = \pi \left[\left(\frac{n_x}{L_x} \right)^2 + \left(\frac{n_y}{L_y} \right)^2 + \left(\frac{n_z}{L_z} \right)^2 \right]^{1/2} \tag{3.26}$$

Here, n_x, n_y, n_z are mode numbers in x-, y- and z-direction respectively and L_x, L_y, L_z denote room dimensions in meters along x-, y- and z-direction respectively.

If “the average spacing” between mode frequencies is larger than “the average half-width” which is the bandwidth (in Hertz) of a resonance curve -3 dB below its maximum value (i.e. half power) room resonances can be treated separately [14]. This frequency range is governed by discrete room modes. On the other hand, if the average spacing between mode frequencies is considerably smaller than “the average half-width of resonances”, then a large number of normal modes influences the sound pressure in this frequency region and room resonances can not be treated separately. In this frequency range room exhibits a reverberant behavior. A restriction that separates these two different behaviors of a room is stated by Schroeder. According to him, the frequency where three times of the average spacing between normal modes covered by the average bandwidth of resonances is the limiting frequency separating these conditions. That frequency can be estimated by using the following formula [14]:

$$f_s = \left[3 \times \frac{c^3}{4\pi V \left(\langle \delta_n \rangle / \pi \right)} \right]^{1/2} \tag{3.27}$$

where, f_s is the limiting frequency (Schroeder frequency), c is the speed of sound (m/s), V is the volume of the room (m^3) and $\langle \delta_n \rangle / \pi$ represents the average band-width of the resonances.

If the speed of sound is taken $c = 340$ m/s and the reverberation time is expressed as $T = \frac{6.91}{\langle \delta_n \rangle}$ then the Schroeder frequency becomes [14]:

$$f_s \approx 2000\sqrt{\frac{T}{V}} \tag{3.28}$$

Considering the accuracy of the reverberation room measurements, especially at low frequencies it is very difficult to obtain accurate measurement results because of the "insufficient modal density of the reverberation room" [3]. In practice, to obtain more uniform normal mode frequency distribution, especially in the low frequency bands, room dimensions should not be in the ratio of integers [3].

3.7 Calculations

The equivalent absorption areas of the reverberation room without and with the test specimen A_1 and A_2 respectively are calculated by using the formulae given below [3]:

$$A_1 = 55.3\frac{V}{c_1 T_1} - 4Vm_1 \tag{3.29}$$

$$A_2 = 55.3\frac{V}{c_2 T_2} - 4Vm_2 \tag{3.30}$$

The absorption coefficient was defined before as the ratio of the equivalent absorption area of the specimen A_T which is equal to the value of $(A_2 - A_1)$ to the

area of the specimen S. So, this will lead us to the equations used in the calculations of the absorption coefficients given below as defined in ISO 17497-1 [1, 3]:

Random-incidence absorption coefficient (α_s):

$$\alpha_s = 55.3\frac{V}{S}\left(\frac{1}{c_2 T_2} - \frac{1}{c_1 T_1}\right) - \frac{4V}{S}(m_2 - m_1) \tag{3.31}$$

Random-incidence specular absorption coefficient (α_{spec}):

$$\alpha_{spec} = 55.3\frac{V}{S}\left(\frac{1}{c_4 T_4} - \frac{1}{c_3 T_3}\right) - \frac{4V}{S}(m_4 - m_3) \tag{3.32}$$

The random incident scattering coefficient is expressed in the previous chapter as one minus the ratio of the energy reflected in specular manner to the incident energy. After rearranging the equation (1.1)

$$s = \frac{E_{r,scat}}{E_{r,total}} = \frac{(E_{r,scat} + E_{abs}) - E_{abs}}{E_i - E_{abs}} \tag{3.33}$$

the numerator and the denominator of the obtained expression are divided by E_i and submission of equations (1.2) and (1.3) into this new expression results in the random-incidence scattering coefficient (s):

$$s = 1 - \frac{1-\alpha_{spec}}{1-\alpha_s} = \frac{\alpha_{spec} - \alpha_s}{1-\alpha_s} \tag{3.34}$$

where V is the volume of the reverberation room in m^3, S is the area of the test sample in m^2. T_1 and T_2 denote reverberation times in seconds without and with

the sample as turntable is not rotating, respectively. T_3 and T_4 stand for reverberation times in seconds without and with the sample while turntable is rotating, respectively. c_1, c_2, c_3 and c_4 define the speed of sound in air, m/s, and m_1, m_2, m_3 and m_4 stand for energy attenuation coefficients of air in reciprocal meters during the measurements of T_1, T_2, T_3 and T_4, respectively.

The speed of sound in the air c and the energy attenuation coefficient m are calculated by using the formulae below [1]:

$$c = 343.2\sqrt{\frac{273.15+T}{293.15}} \tag{3.35}$$

$$m = \frac{\alpha}{10\log(e)} \tag{3.36}$$

Here, T stands for the air temperature in degrees Celsius and α indicates the sound pressure attenuation coefficient. The calculation procedure for the sound pressure attenuation coefficient α is described in the corrections for results section.

In addition to these coefficients scattering coefficient of the base plate should be calculated too because of the restriction about this quantity stated in ISO 17497-1 using the formula below [1]:

$$s_{\text{base}} = 55.3\frac{V}{S}\left(\frac{1}{c_3T_3} - \frac{1}{c_1T_1}\right) - \frac{4V}{S}(m_3 - m_1) \tag{3.37}$$

3.8 Factors Influence the Accuracy and Corrections for Results

The temperature and humidity of the air filling the room are two very important properties that affect the measurement accuracy [1]. Since these two quantities have a great influence on the propagation of sound in a medium, they should be kept invariant as far as possible and recorded before and after measurements to make some corrections for air attenuation within the room especially at high frequencies [1, 3]. Their mean values are used in the calculation of the attenuation coefficient α (in decibel per meter) as described in ISO 9613-1 and shown below [15]:

$$\begin{aligned}\alpha = 8.686\, f^2([1.84\times10^{-11}\left(\frac{p_a}{p_r}\right)^{-1}\left(\frac{T}{T_0}\right)^{1/2}]+ \\ (\frac{T}{T_0})^{-5/2}\times\{0.01275[\exp(\frac{-2239.1}{T})][f_{rO}+(\frac{f^2}{f_{rO}})]^{-1}+ \\ 0.1068[\exp(\frac{-3352.0}{T})][f_{rN}+(\frac{f^2}{f_{rN}})]^{-1}\})\end{aligned} \tag{3.38}$$

where the relaxation frequencies of oxygen and nitrogen, f_{rO} and f_{rN} respectively are found by using:

$$f_{rO} = \frac{p_a}{p_r}(24 + 4.04\times10^4 h\frac{0.02+h}{0.391+h}) \tag{3.39}$$

and

$$f_{rN} = \frac{p_a}{p_r}(\frac{T}{T_0})^{-1/2}\times(9+280h\,\exp\{-4.170[(\frac{T}{T_0})^{-1/3}-1]\}) \tag{3.40}$$

Here, f is center frequency of the related one-third octave band in s^{-1}. p_a and p_r denote ambient atmospheric pressure inside the room in kPa and the reference

atmospheric pressure (101.325 kPa), respectively. T and T_0 stand for mean air temperature inside the room and reference air temperature in Kelvin, respectively. h ,is molar concentration of water vapor in percent.

The value of molar concentration of water vapor h is estimated by using the formula:

$$h = h_r \frac{\left(\frac{p_{sat}}{p_r} \right)}{\left(\frac{p_a}{p_r} \right)} \tag{3.41}$$

where

$$\frac{p_{sat}}{p_r} = 10^C \tag{3.42}$$

for

$$C = -6.8346 \left(\frac{T_{01}}{T} \right)^{1.261} + 4.6151 \tag{3.43}$$

where, h_r is mean relative humidity of the air inside the room in percents, p_{sat} is saturation vapor pressure in kPa and T_{01} is the triple-point isotherm temperature of 273.16 K.

Moreover, any air movement within the room should not be allowed to keep the medium as time-invariant as possible [1]. Hence, the reverberation room should be left at rest before the measurements to minimize the unstable conditions possibly existing within the room.

CHAPTER 4

CEPSTRAL DECONVOLUTION

4.1 Introduction

For an arbitrary composite signal $x(t)$ its cepstrum function describes the spectrum of a logarithmic spectrum of this signal. This function is very powerful because if this signal is composed of a basic wavelet (e.g. an excitation signal) and a periodic component (e.g. due to its echoes), logarithm of the spectrum of this signal shows the delayed echoes as ripples. Then the spectrum of this logarithmic spectrum gives the frequency of these ripples in the form of peaks at echo delay times [16, 17].

The term cepstrum is derived from the term spectrum via a syllabic interchange to avoid the confusion between the spectral and the cepstral properties [16]. The same change is applied also for other spectral terms for cepstral counterparts such as quefrency (frequency), liftering (filtering) etc.

Oppenheim and Schafer describe the cepstrum as "a fundamental part of the theory of homomorphic systems for processing signals that have been combined by convolution" [17]. They also call the procedure for the calculation of the cepstrum of a signal as a homomorphic transformation. Because homomorphic systems provide a generalized use of the superposition principle in algebraic operations, cepstrum analysis uses the same principles of superposition in algebraic operations. For example, the deconvolution procedure of a combined signal (superimposed in terms of convolution of the input signal and its echoes) is

done by just addition and subtraction operations in cepstral domain. This is called as cepstral or more generally homomorphic deconvolution.

Cepstrum techniques are widely used for echo detection and signal decomposition. These two issues form the basic structure of a deconvolution process. Considering a signal which is composed of multiple signals overlapped in time domain, deconvolution process starts with determination of the echoes in the signal in terms of their relative amplitudes and epochs (arrival or delay times) by employing real (or power) cepstrum. Then, complex cepstrum is calculated for this signal and undesired parts of the signal are removed via filtering in cepstral domain. Finally, reconstruction of the remaining signal is done by transformation back to the time domain.

4.1.1 Real and Power Cepstrum

Power cepstrum of an arbitrary function $x(t)$ may be defined as the inverse Fourier transform of the logarithm of the power spectrum of this function. Power spectrum of the function can be obtained by using the formula [14]

$$S_{xx}(\omega) = \lim_{T_0 \to \infty} \left[\frac{1}{T_0} X_{T_0}(\omega) X_{T_0}^*(\omega) \right] \tag{4.1}$$

where $X_{T_0}(\omega)$ and $X_{T_0}^*(\omega)$ denote the Fourier transform of the $x(t)$ function and its complex conjugate, respectively. Then, the power cepstrum can be shown as below [18]

$$c_{p,x}(\tau) = F^{-1}\left\{ \log\left(S_{xx}(\omega) \right) \right\} \tag{4.2}$$

Different from power cepstrum, real cepstrum of an arbitrary function $x(t)$ can be described as the inverse Fourier transform of the logarithm of the magnitude

of the Fourier transform of this function. Real spectrum of the function can be obtained by using the formula below

$$c_{r,x}(\tau) = F^{-1}\left\{\log\left(\left|F\left\{x(t)\right\}\right|\right)\right\} = F^{-1}\left\{\log\left|X(\omega)\right|\right\} \tag{4.3}$$

As mentioned above the delay times and amplitudes of echoes are determined by using real (or power) cepstrum easily. However, because all of the phase information of the signals is lost during the calculation, it is impossible to reconstruct the separated signals through power cepstrum.

4.1.2 Complex Cepstrum

Complex cepstrum of an arbitrary function $x(t)$ may be defined as the inverse Fourier transform of the logarithm of the Fourier transform of this function.

$$c_c(\tau) = F^{-1}\left\{\log\left[F\left\{x(t)\right\}\right]\right\} = F^{-1}\left\{\log\left[X(\omega)\right]\right\} \tag{4.4}$$

Complex cepstrum is employed for separation of the components of the composite waveforms, especially combined via convolution. Different from the real and power cepstrum, phase information of the signals is kept in the complex cepstrum. So, it can be utilized in the reconstruction of the separated parts

It is also possible to determine delay times with employing complex cepstrum. However, any linear phase component with a large slope possibly existing in the signal may dominate the cepstrum. Therefore, it could be impossible to estimate the delay times accurately [19].

4.2 Cepstral Deconvolution

4.2.1 General

Cepstral deconvolution for a composite signal $x(t)$ is achieved in three steps, namely,

i) Estimation of the echo delay times in cepstral domain by employing real (or power) cepstrum of the signal,

ii) Evaluation of the complex cepstrum of the signal and removal of the unwanted parts in the cepstral domain via linear filtering,

iii) Restoration of the desired part of the signal in time domain by reversing the procedure followed in the calculation of the complex cepstrum.

Consider an arbitrary signal $x(t)$ which is the result of two convolved signals

$$x(t) = x_1(t) * x_2(t) \tag{4.5}$$

Firstly, both sides of the above expression are Fourier transformed. Then it becomes

$$\begin{aligned} X(\omega) &= X_1(\omega) \cdot X_2(\omega) \\ &= \left[X_1 e^{j\omega} \right] \cdot \left[X_2 e^{j\omega} \right] \end{aligned} \tag{4.6}$$

At this point one can estimate the real cepstrum by taking inverse Fourier transform of the logarithm of the magnitudes of the complex expressions above

$$
\begin{aligned}
c_{r,x}(\tau) &= F^{-1}\left\{\log\left(|X_1|\cdot|X_2|\right)\right\} \\
&= F^{-1}\left\{\log|X_1| + \log|X_2|\right\} \\
&= \hat{x}_{r,1}(\tau) + \hat{x}_{r,2}(\tau)
\end{aligned} \tag{4.7}
$$

It should be noted that the index r is used to indicate the real cepstrum to avoid confusion with complex cepstrum.

In order to estimate the complex cepstrum inverse Fourier transform is applied to the logarithm of the complex expression in equation (4.6)

$$
\begin{aligned}
c_{r,x}(\tau) &= F^{-1}\left\{\log\left(\left[X_1 e^{j\omega}\right]\cdot\left[X_2 e^{j\omega}\right]\right)\right\} \\
&= F^{-1}\left\{\log X_1(\omega) + \log X_2(\omega)\right\} \\
&= \hat{x}_1(\tau) + \hat{x}_2(\tau)
\end{aligned} \tag{4.8}
$$

Let the required part of the signal be $x_1(t)$. To eliminate the undesired part, i.e. $x_2(t)$, the composite signal is filtered in cepstral domain by employing a linear filter $l(\tau)$ which is designed (or selected) due to the delay information obtained from the real cepstrum. Finally, the remaining part of the signal is reconstructed in time domain by reversing the procedure followed from time domain up to cepstral domain

$$
\begin{aligned}
x_1(t) &= F^{-1}\left\{\exp\left(F\left\{c_{r,x}(\tau)\cdot l(\tau)\right\}\right)\right\} = F^{-1}\left\{\exp\left(F\left\{\hat{x}_1(\tau)\right\}\right)\right\} \\
&= F^{-1}\left\{\exp\left(\log X_1(\omega)\right)\right\} \\
&= F^{-1}\left\{X_1(\omega)\right\}
\end{aligned} \tag{4.9}
$$

In practice, the composite signal is usually found in discrete form i.e. $x[n]$. Therefore the corresponding Fourier transforms should be done by using N point DFT (Discrete Fourier Transform). And the number N should be kept as large as

possible to reduce the effects of aliasing in the computation of the complex cepstrum [17].

4.2.2 Deconvolution of Scattering Part from Impulse Response

Components forming an impulse response can be classified into two groups: scattered part and specular part. As mentioned in Chapter 3, specular parts of impulse responses for a particular measurement are highly correlated though their scattered parts are not correlated and even completely independent from each other. It is anticipated that such correlation properties of impulse responses can be used to separate the scattered parts from the rest of the impulse responses via cepstral deconvolution.

Waveforms of the specular parts of impulse responses remain unchanged throughout a particular measurement i.e. not dependent on orientation of the specimen being tested. Then real cepstrum of a series of impulse responses gives specular part of every impulse response in a form of peaks in cepstral domain. Since, cepstral analysis is sensitive to similarity existed in wave structures like the similarity between a basic signal and its successive echoes. And in this case the very first impulse response corresponds to basic signal and specular parts of the rest of the impulse responses correspond to echoes of this basic signal. These specular components can be determined in cepstral domain by indicating evenly separated peaks because every impulse response has the same length and synchronous with each other.

In the application of this approach, impulse responses are added successively. Average of the corresponding series is used as the very first element of this sequence. This is because; average of a series includes all necessary information about the specular parts of impulse responses and also carries less distortion caused by the scattered parts. After applying real cepstrum to this sequence every impulse response after the first one cause a peak in the cepstral domain. Then

deconvolution is achieved by liftering (i.e. filtering in cepstral domain) these peaks employing a linear notch filter. Liftered sequence is transformed into the time domain and this final signal gives specular part free impulse response sequence except the average one located at the beginning of the sequence. This deconvolved signal is subtracted from the original (not deconvolved one) and finally specular parts of the impulse responses are obtained. In the rest of the calculations average of these specular parts of the impulse responses is used in order to increase the signal-to-noise ratio and so accuracy of the measurement.

CHAPTER 5

EXPERIMENTAL SETUP AND RESULTS

In this chapter, the experimental setup (including reverberation room, equipments and test materials) used in experiments and data evaluation procedures for both ISO method and cepstral deconvolution method are described. Moreover, results of the measurements for absorption and scattering coefficients for different specimens are presented for these methods. All of the coefficients are estimated for four different reverberation times which are resulted from the evaluation of decay curves for different evaluation ranges. Results obtained from these different ranges are indicated with different colors on the graphs such that T_{10} is colored in blue and T_{15}, T_{20} and T_{30} are colored in black, green and red, respectively.

5.1 Test Materials

In this study five different materials of square shape with different surface pattern have been used as test specimen in the reverberation room. Although these materials are commercial acoustical panels which are produced for different acoustic treatment purposes and their absorption performances are specified by the producer, these values could not be used for comparison purposes. Because the reverberation room used in the tests is a scaled reverberation room and the results obtained from the measurements correspond to the response of a material which has dimensions larger than the measured one by a factor of scale ratio i.e. 10. These materials are shown below with their commercial names:

Figure 5.1 - Specimen 1: Reflector Panel YST-KNL/3x5 Lake

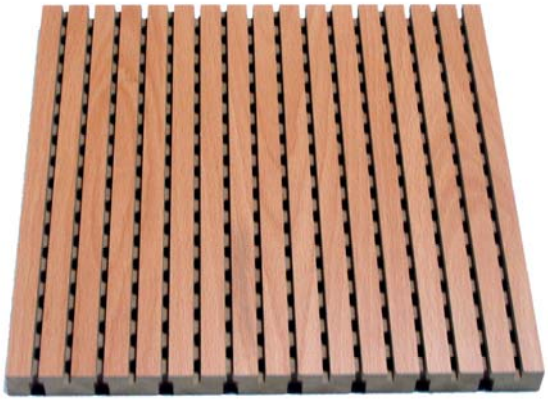

Figure 5.2 - Specimen 2: Mid-Frequency Panel KP4000DS

Figure 5.3 - Specimen 3: Low-Frequency Panel LM2000DS

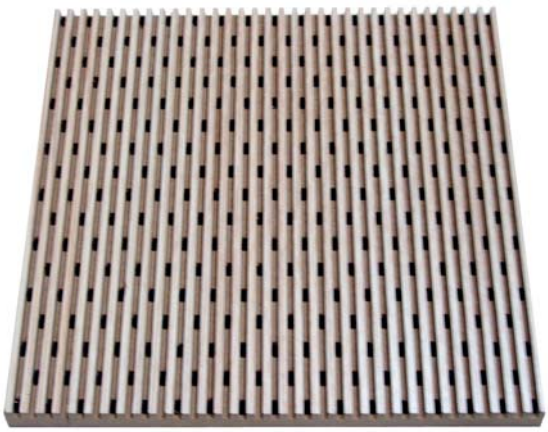

Figure 5.4 - Specimen 4: High-Frequency Panel LM4000DS

Figure 5.5 - Specimen 5: Mid-Frequency Panel LM1000DS

5.2 Test Equipment and Signal

In order to conduct measurements a physically scaled reverberation room with a scale ratio of 1:10 has been built according to the standards ISO 17497-1 and ISO 354. Therefore, all the dimensions comply with the requirements of these standards given in Appendix A. Walls of the reverberation room are made of Plexiglas (Degussa Plexiglas GS series, 20 mm in thickness) and the base plate of the turntable is produced using MDF (medium density fibreboard). Rotational movement of the base plate is achieved by a 12 V DC motor (Crouzet 82 861 014). Specifications of the room are given in Table 1:

Table 5.1 – Specifications of the reverberation room

Reverberation room	
Length	0.72 m
Width	0.6 m
Height	0.465 m
Volume	0.201 m^3
Turntable	
Diameter of the base plate	0.38 m
Rotational speed of the base plate (the motor operating at 3 V)	0.364 rpm

A maximum length sequence (MLS) of order 16 is used to construct the test (excitation) signal. The angular speed of the turntable and length of the MLS were taken into account to generate the signal by successive addition of 1+120 basic sequence (1^{st} sequence will be dropped in the evaluation of the output signal due to the need for reaching a steady sound pressure level at first). This final sequence is sampled with frequency of 48 kHz and recorded as a sound wave in PC environment by using MATLAB. The recorded test signal is then sent to the loudspeakers (a pair of LS hi-fi tweeter with nominal impedance of 8 ohm) by a soundcard (SoundBlaster Live Value) and an integrated amplifier (Marantz PM4001). In order to collect the signal involving the impulse response of the reverberation room, a ¼″ pressure microphone (G.R.A.S. 40 BP) is employed. Finally, this signal is recorded by using the same soundcard after the signal is amplified through B&K preamplifier Type 2639 with B&K microphone power supply Type-2807. The flowchart of the measurement procedure over the test equipment is shown in Figure 5.10.

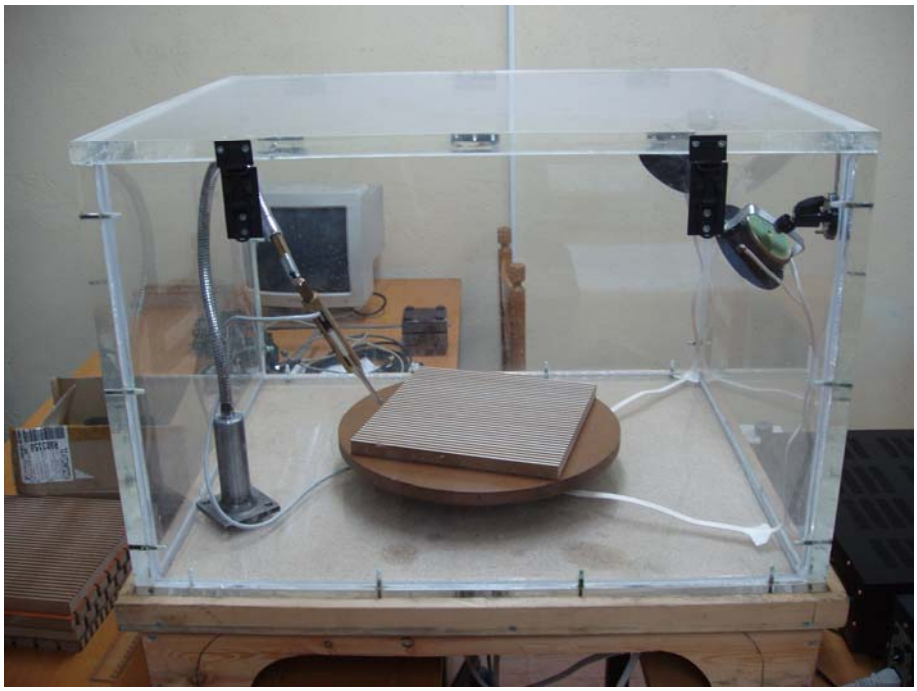

Figure 5.6 – The reverberation room (front view)

Figure 5.7 – Bottom view of the reverberation room and the DC motor

Figure 5.8 – Microphone and preamplifier attached to the holder (left) and one of the loudspeakers (right)

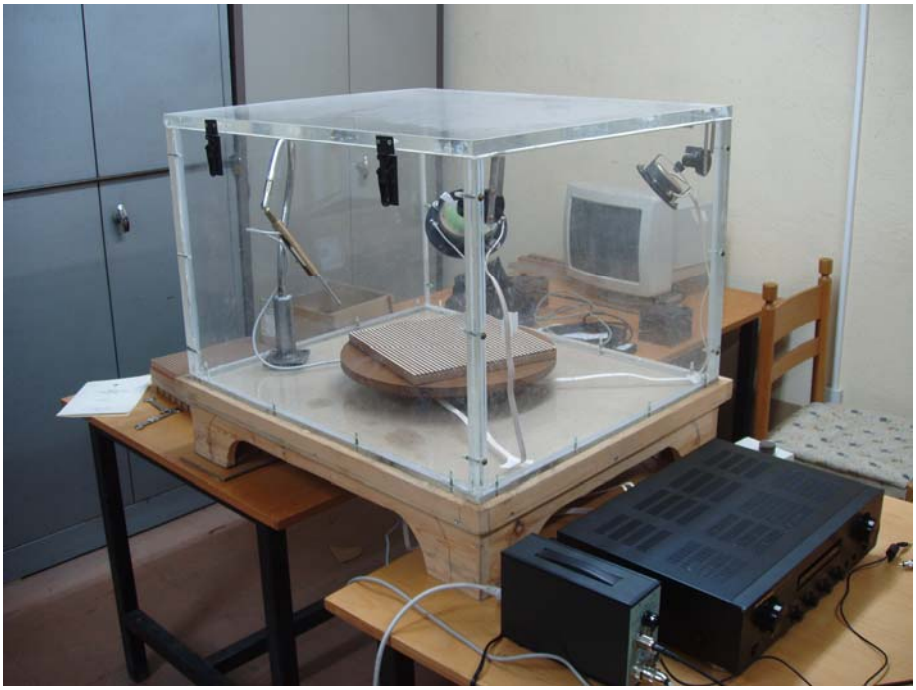

Figure 5.9 – Measurement setup with microphone power supply and integrated amplifier

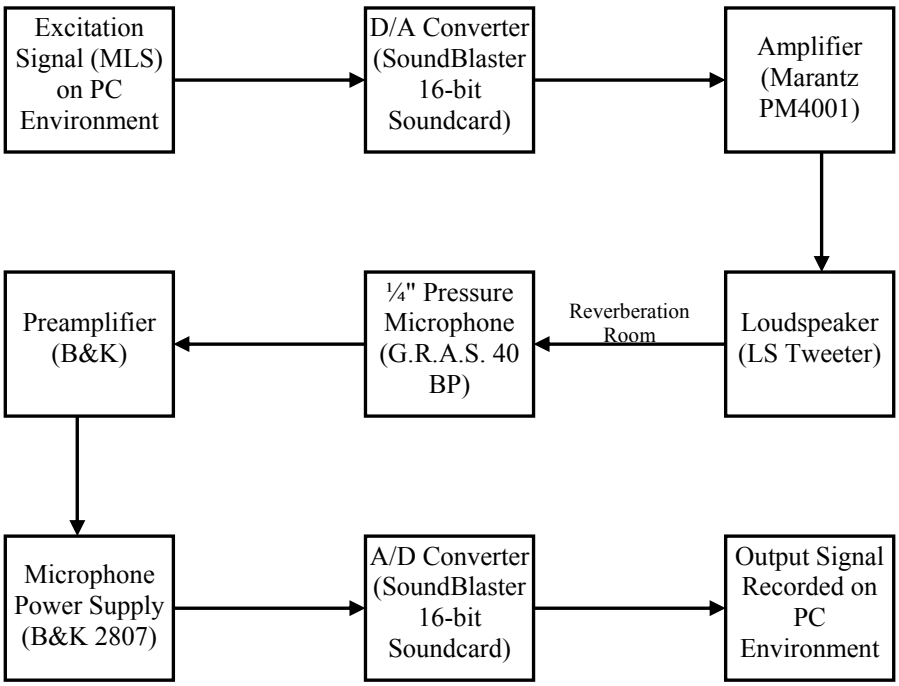

Figure 5.10 – Flowchart of the measurement procedure

5.3 Test Procedure

In measurements, total of six combinations of two loudspeaker and three microphone position are used for testing each material (see Table 5.2 and Figure 5.11). Every material is tested for each loudspeaker/microphone position combination for four different reverberation times (T_1, T_2, T_3, T_4), i.e. 24 measurements are carried for each material. Test procedure is as follows

I. Material to be tested is placed (or removed according to requirement of reverberation time to be measured) into the reverberation room, microphone and loudspeaker positions are arranged, temperature, pressure and relative humidity of the room is measured, and the room is closed,
II. Turntable is operated (or stopped according to requirement of reverberation time to be measured),
III. It should be ensured that steady state conditions in the room is established (it takes about 2 minutes for the room considered),
IV. Test signal is started to play and recording is initiated simultaneously,
V. When the test is completed recording of the signal is stopped.

Table 5.2 – Microphone and loudspeaker positions

Distance from / **Position of**	**Front Wall**	**Nearest Side Wall**	**Floor (Height)**
Microphone 1	150 mm	230 mm	200 mm
Microphone 2	300 mm	170 mm	180 mm
Microphone 3	490 mm	250 mm	180 mm
Loudspeaker 1	50 mm	80 mm	400 mm
Loudspeaker 2	550 mm	80 mm	400 mm

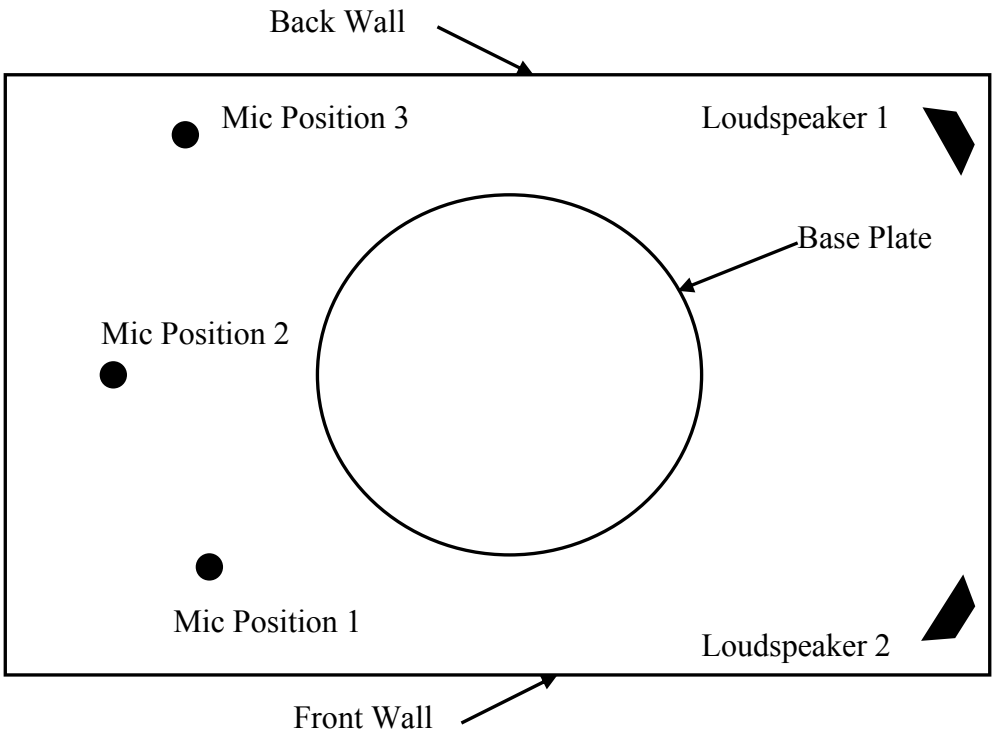

Figure 5.11 – Microphone and loudspeaker positions from the top view of the reverberation room

5.4 Evaluation Procedure and Results for ISO Method

In this section, firstly evaluation procedure applied on the recorded output data according to ISO method is explained. Then, results for random-incidence absorption and scattering coefficients obtained through this procedure are demonstrated in graphical form.

5.4.1 Evaluation Procedure

A MATLAB code is written in order to determine reverberation times and absorption and scattering coefficients of the material from the recorded signal. Evaluation procedure is described below

I. The recorded signal is imported to the MATLAB,
II. Signal is separated into parts (i.e. total number of 120) with respect to the length of the MLS (see Figure 5.12),
III. Room impulse response corresponding for each maximum length sequence is evaluated by deconvolving the input signal (MLS) from the recorded output signal via employing Fast Hadamard Transform,
IV. Average of impulse responses is calculated,
V. Averaged impulse response is filtered in frequency domain by using 1/3 octave band-pass filters (designed in MATLAB Filter Analysis and Design Toolbox with Butterworth filter characteristics),
VI. Backward integration is applied after squaring the impulse response in time domain to obtain energy decay curve,
VII. Reverberation times are calculated from the energy decay curve. First of all least squares fit algorithm is applied on initial part of the decay where the evaluation is done. Then, from these straight lines corresponding reverberation times are estimated. Normalized sound pressure level values of -5 dB and -15 dB, -20 dB, -25 dB and-35 dB on the decay curve has been used as evaluation ranges to obtain T_{10}, T_{15}, T_{20} and T_{30} respectively.
VIII. Step I to VII is repeated for each 24 measurement signal acquired for the corresponding material and the reverberation times obtained are averaged in spatial manner,
IX. Using averaged reverberation times, absorption and scattering coefficient of the materials and scattering coefficient of the base plate of the turntable is determined.

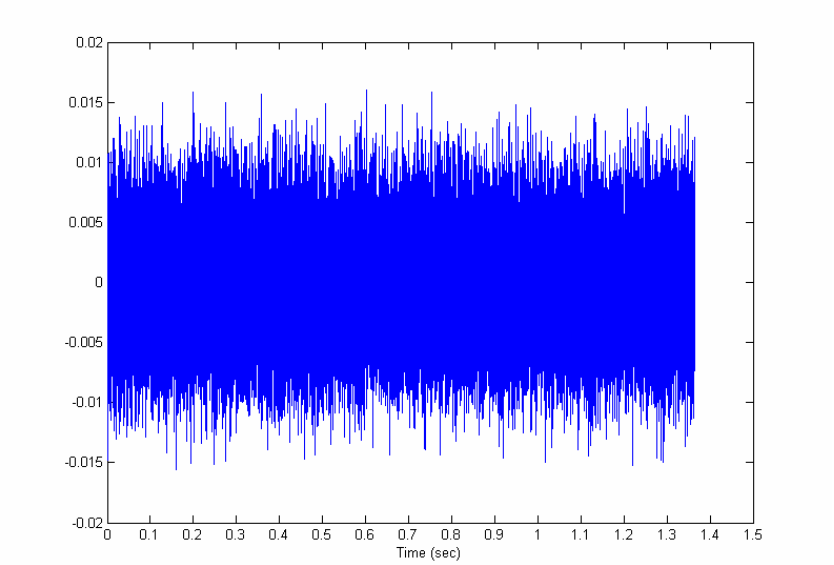

Figure 5.12 – A separated part of the signal recorded with a duration of a period of the MLS signal of order 16

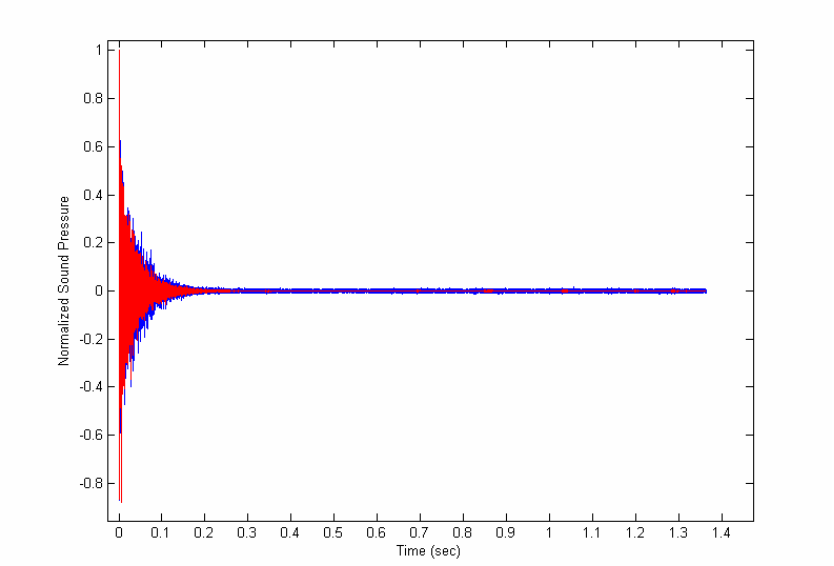

Figure 5.13 – A broadband impulse response (blue) obtained by applying FHT to the output signal shown in Figure 5.12 and the average impulse response (red) for this measurement set

5.4.2 Results

Absorption and scattering coefficients of the specimens obtained according to ISO method are illustrated in the following graphs (Figure 5.14 to 5.23).

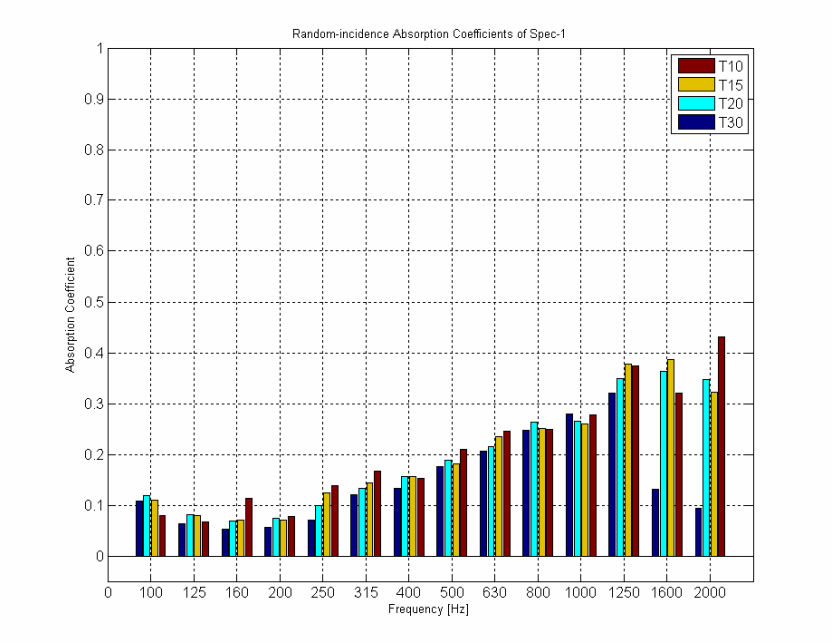

Figure 5.14 – Random-incidence absorption coefficients of specimen 1 (ISO Method)

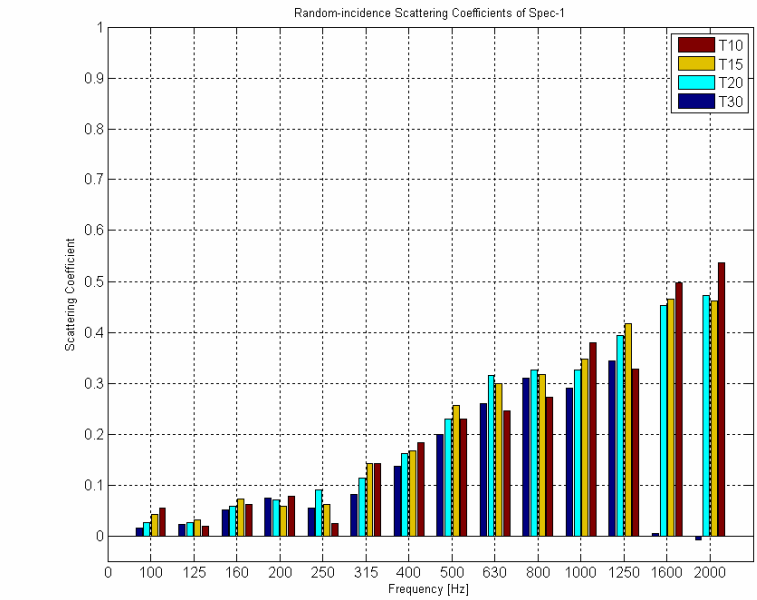

Figure 5.15 – Random-incidence scattering coefficients of specimen 1 (ISO Method)

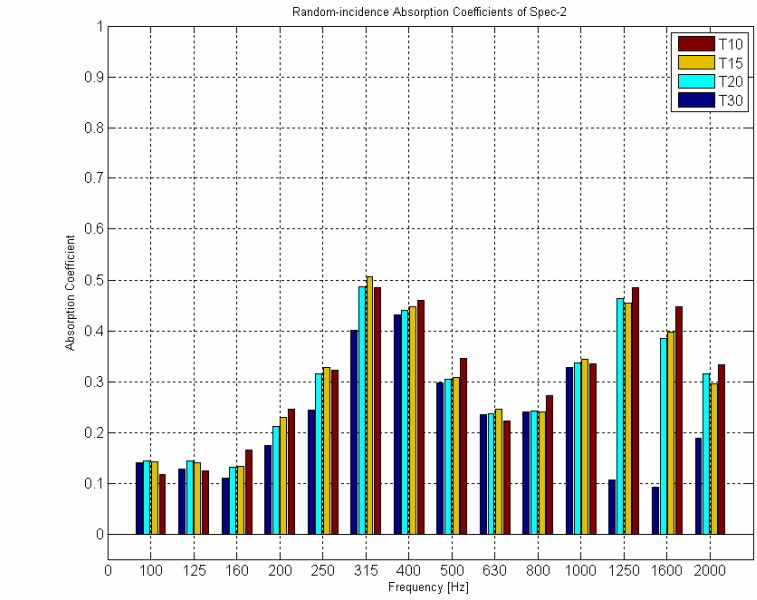

Figure 5.16 – Random-incidence absorption coefficients of specimen 2 (ISO Method)

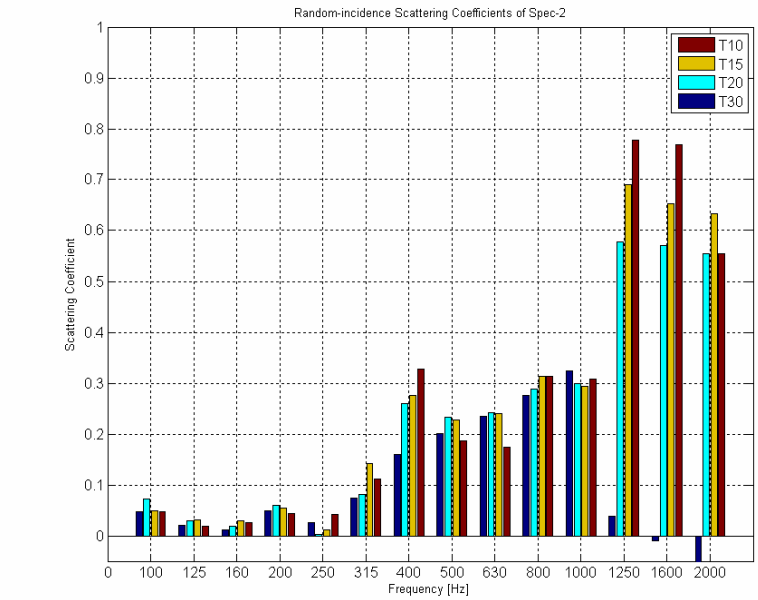

Figure 5.17 – Random-incidence scattering coefficients of specimen 2 (ISO Method)

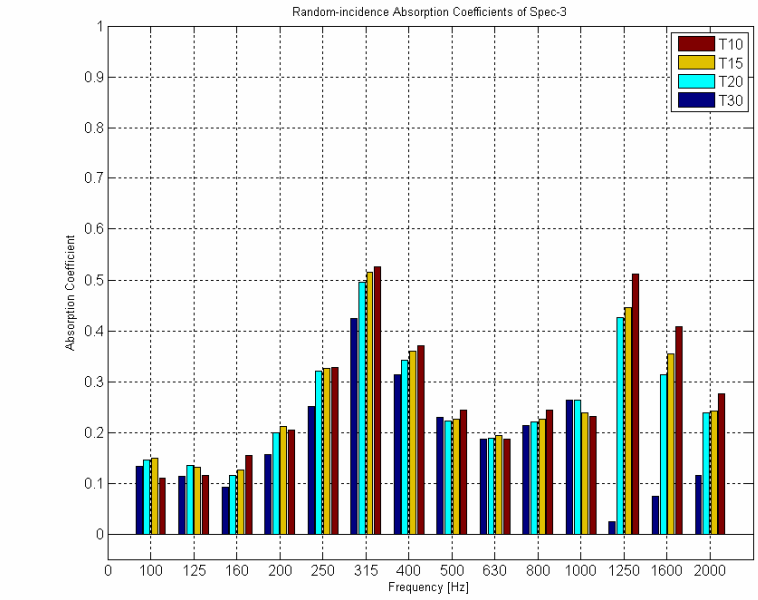

Figure 5.18 – Random-incidence absorption coefficients of specimen 3 (ISO Method)

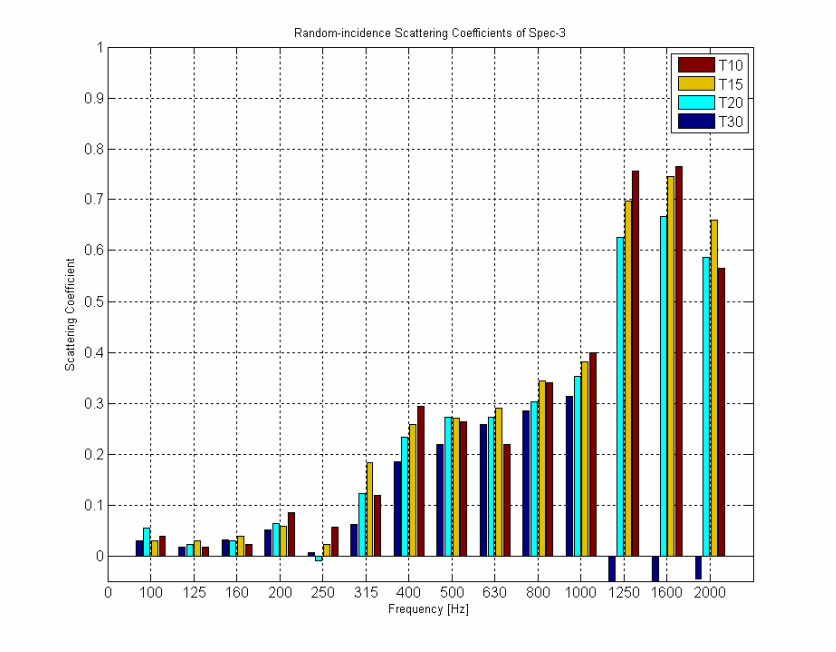

Figure 5.19 – Random-incidence scattering coefficients of specimen 3 (ISO Method)

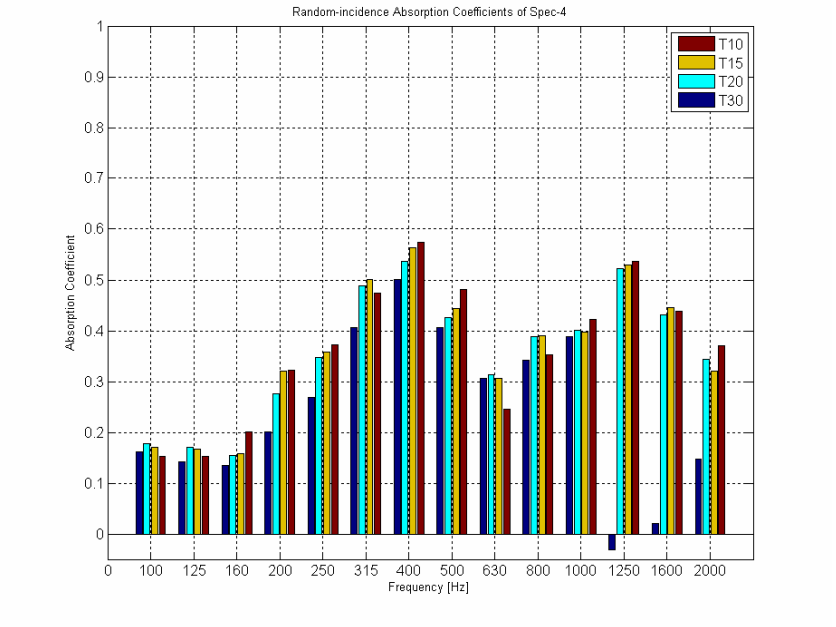

Figure 5.20 – Random-incidence absorption coefficients of specimen 4 (ISO Method)

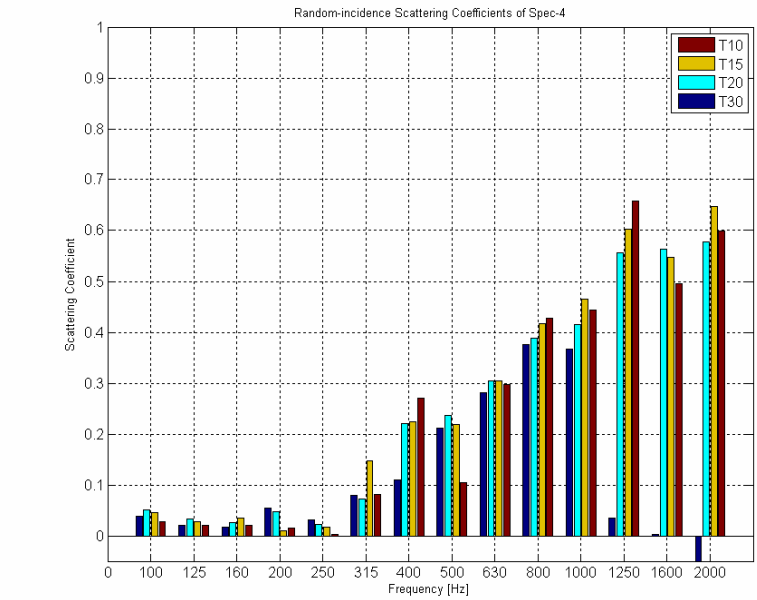

Figure 5.21 – Random-incidence scattering coefficients of specimen 4 (ISO Method)

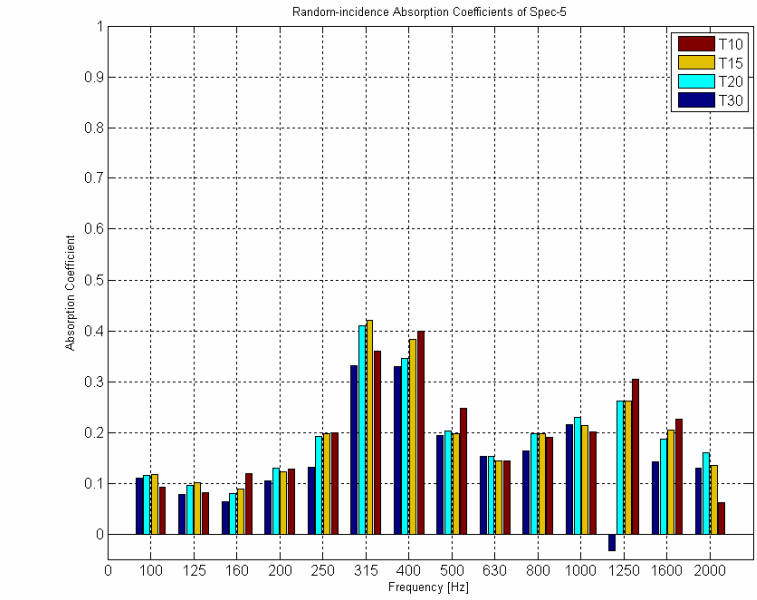

Figure 5.22 – Random-incidence absorption coefficients of specimen 5 (ISO Method)

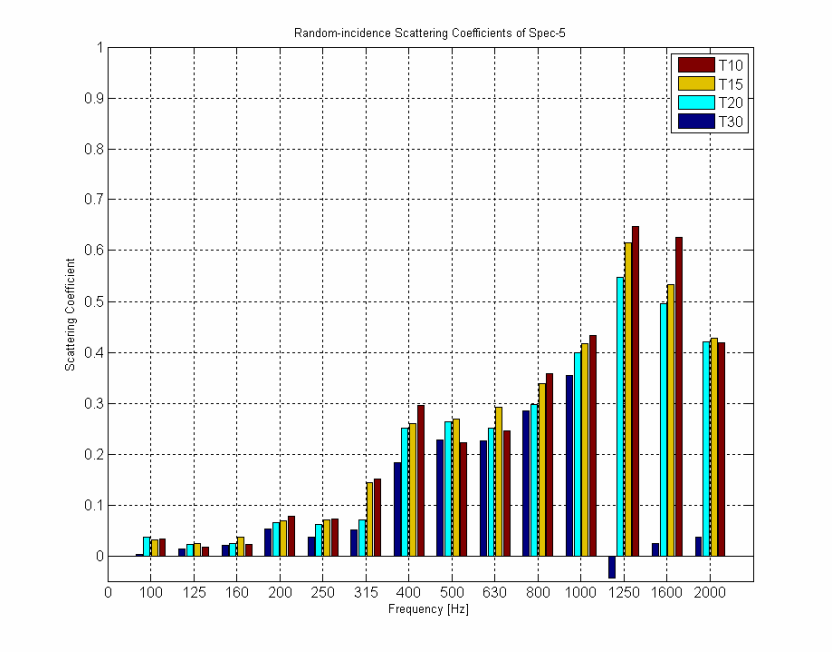

Figure 5.23 – Random-incidence scattering coefficients of specimen 5 (ISO Method)

5.5 Evaluation Procedure and Results for Cepstral Deconvolution

In this part, first of all a simple cepstral deconvolution case which is very similar to the real one is examined using computer generated data in order to present how cepstral deconvolution works. In addition, suitability and accuracy of the deconvolution routine used has been checked on this simple case. Then, the procedure followed in the evaluation of the recorded output data, especially the deviations from the ISO method, is explained. Finally, results obtained for random-incidence absorption and scattering coefficients is presented in graphical form.

5.5.1 Computer Generated Cepstral Deconvolution Case

In this case a damping sinusoidal signal with length of 140 samples has been generated on MATLAB environment and it has been taken as the basic signal.

Then, nine replicas of it have been added successively behind this basic signal (see Figure 5.24). Finally, the total length of the signal has been extended to 50000 samples to reduce cepstral aliasing as much as possible.

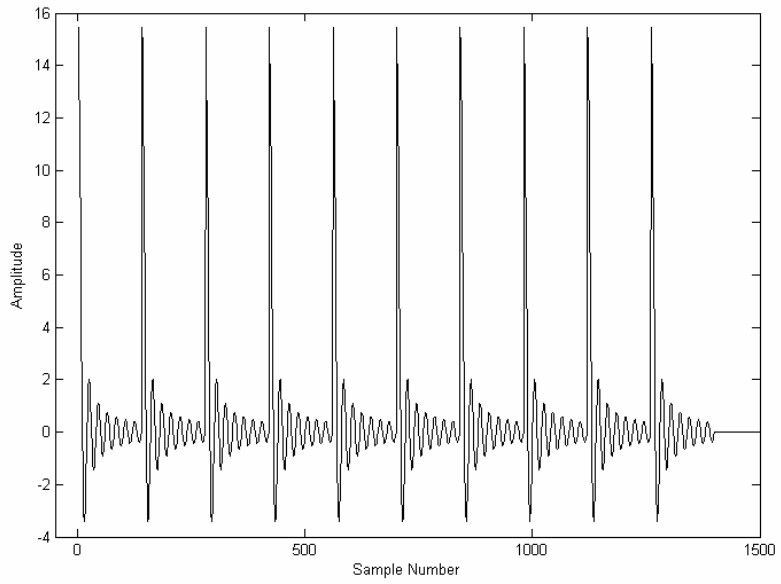

Figure 5.24 – Composite signal (basic signal and its replicas)

First of all the real cepstrum of the signal has been found to indicate the arrival times of echoes, i.e. replicas. As shown in Figure 5.25 the arrival times with respect to the basic signal is located on sample 140 and its integer multiples for other eight replicas and this result is consistent with the expected one. Then, to remove these echoes from the composite signal, complex cepstrum of the composite signal has been estimated (see Figure 5.26). A linear notch filter has been applied to the complex cepstrum on samples where arrival times located such that for samples 140.n for n = 1, 2,…8. By the way, to demonstrate the effect of the notch filter it has been also applied to the real cepstrum as shown in Figure 5.27. Finally, by taking inverse transform of the filtered complex cepstrum of the signal the basic signal is separated from its replicas and *vice versa* (see Figure 5.28).

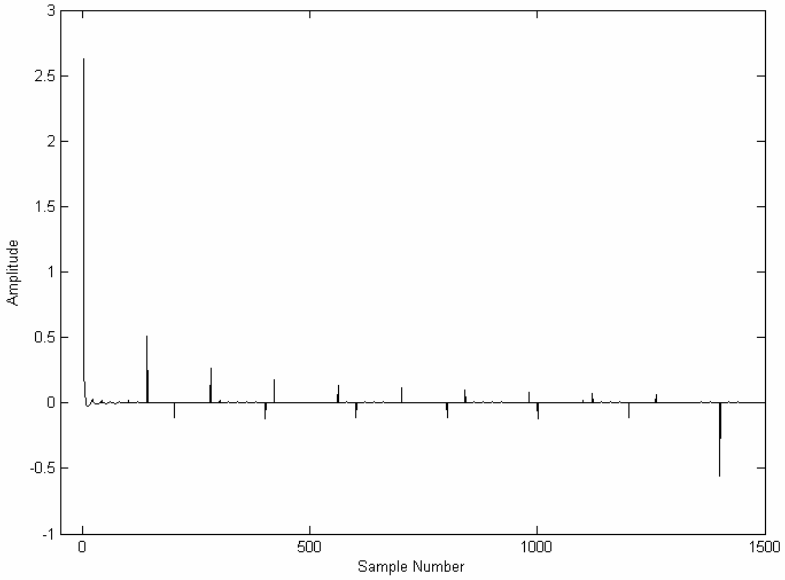

Figure 5.25 – Real cepstrum of the composite signal

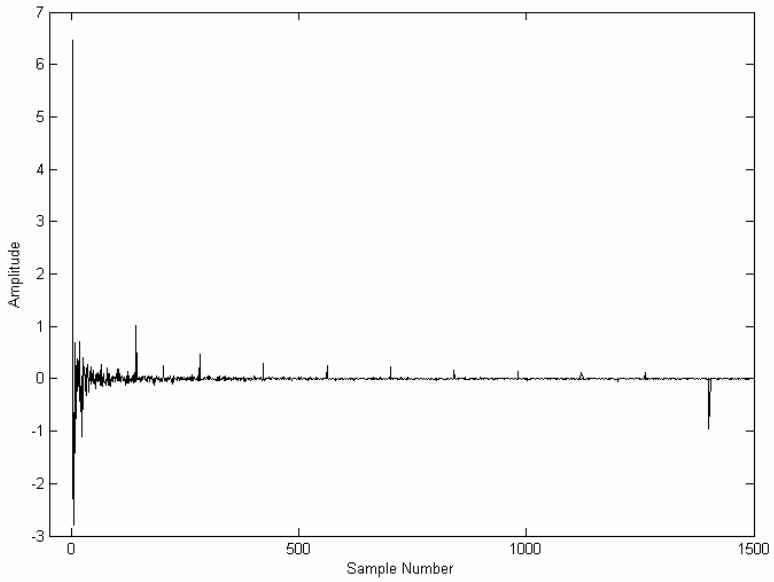

Figure 5.26 – Complex cepstrum of the composite signal

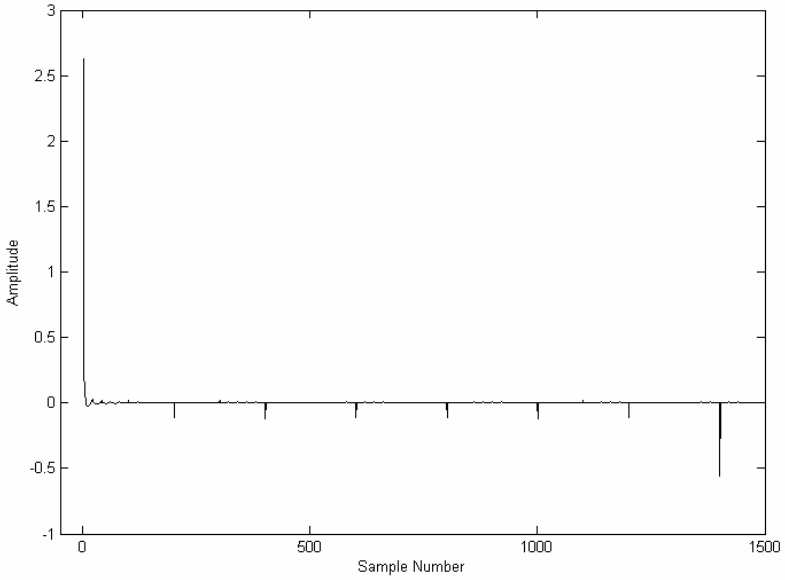

Figure 5.27 – Filtered real cepstrum of the signal

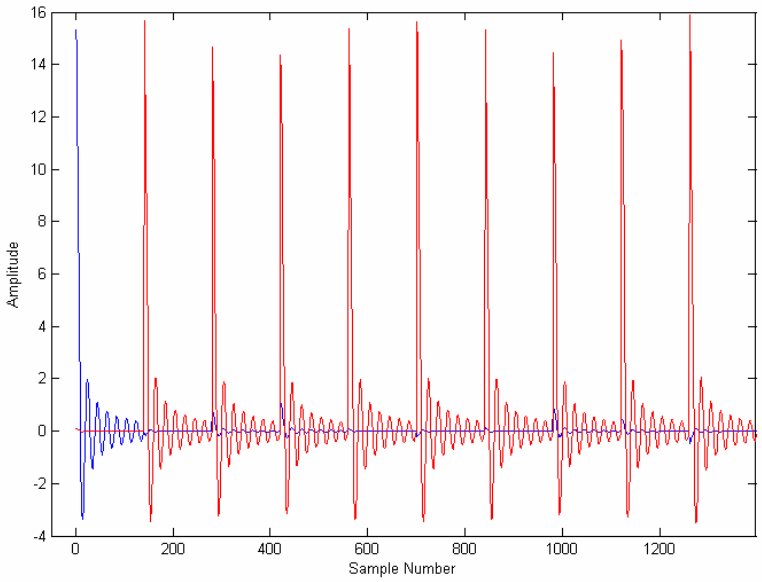

Figure 5.28 – Separated parts of the composite signal: recovered basic signal (blue) and its replicas (red)

5.5.2 Evaluation Procedure

Evaluation procedure for cepstral deconvolution choice is done with a MATLAB subroutine which has been embedded into the code used for the ISO method. In this case specular impulse response is obtained by cepstral deconvolution instead of averaging of impulse responses. All other steps of the evaluation procedure followed in ISO method are left unchanged. Evaluation procedure is explained below:

Evaluation procedure for the ISO method remains same, but between step IV and step V additional tasks listed below are done by the embedded subroutine

I. Separated impulse responses are added successively and averaged impulse response is added to beginning of this sequence,
II. Peak positions which indicate arrival times of specular parts with respect to averaged impulse response are determined by applying real cepstrum to this sequence,
III. Complex cepstrum of the sequence is calculated. Then notch liftering is applied on every peak resulted from impulse responses,
IV. Liftered signal is reconstructed in time domain and it is subtracted from the original (not deconvolved) signal sequence to obtain the specular parts of the impulse responses,
V. Specular parts of the impulse responses are averaged.

5.5.3 Results

Evaluation has been done for 12 evenly separated (i.e. for different orientations of turntable with 30° angular steps) impulse responses out of 120. Absorption and scattering coefficients of the specimens obtained according to cepstral deconvolution method are illustrated in the following graphs (Figure 5.29 to 5.38).

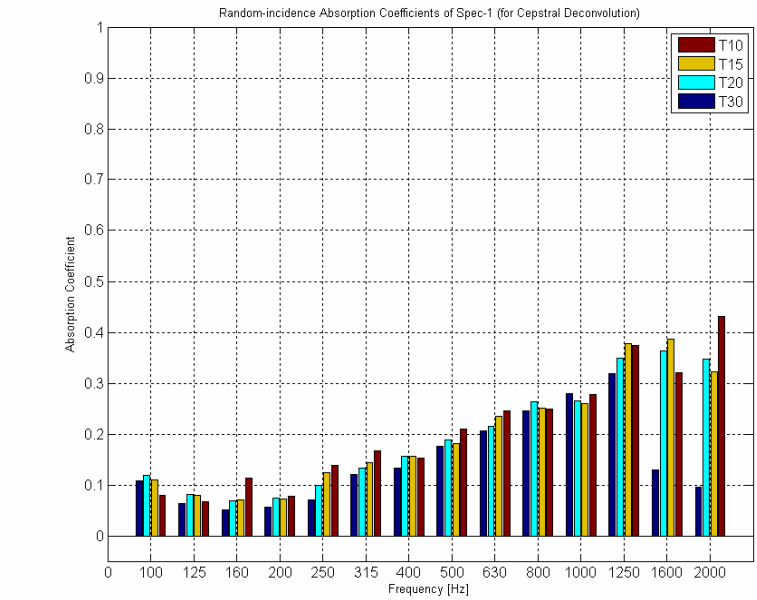

Figure 5.29 – Random-incidence absorption coefficients of specimen 1 (Cepstral Deconvolution)

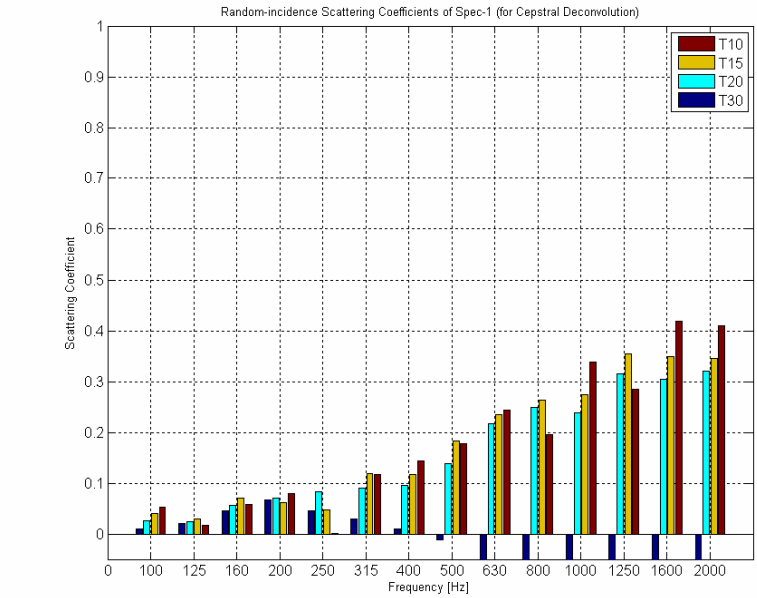

Figure 5.30 – Random-incidence scattering coefficients of specimen 1 (Cepstral Deconvolution)

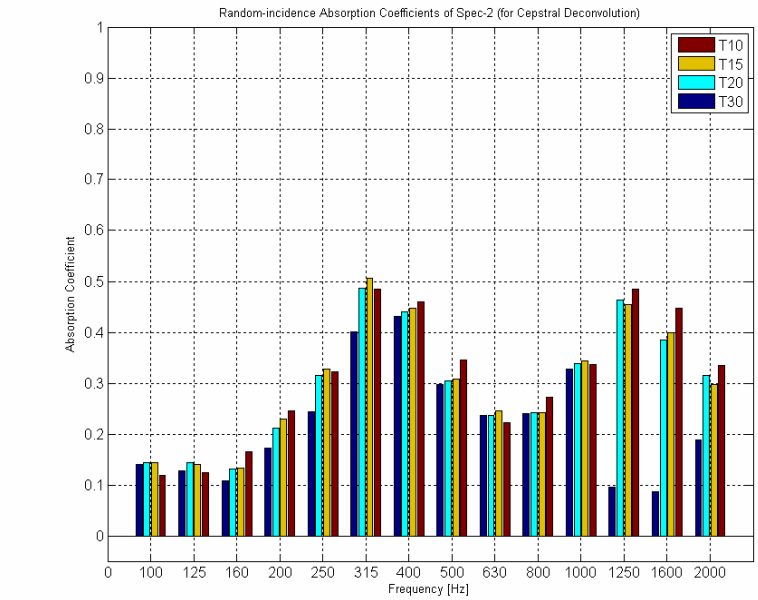

Figure 5.31 – Random-incidence absorption coefficients of specimen 2 (Cepstral Deconvolution**)**

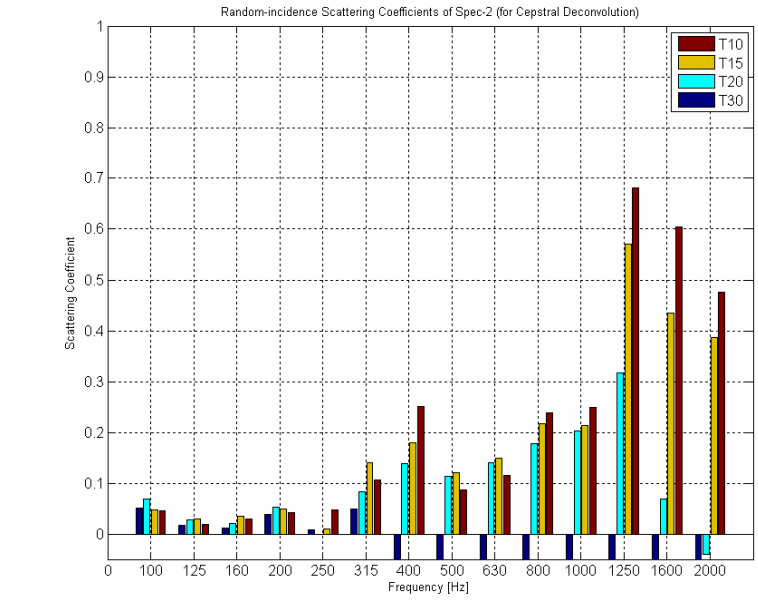

Figure 5.32 – Random-incidence scattering coefficients of specimen 2 (Cepstral Deconvolution)

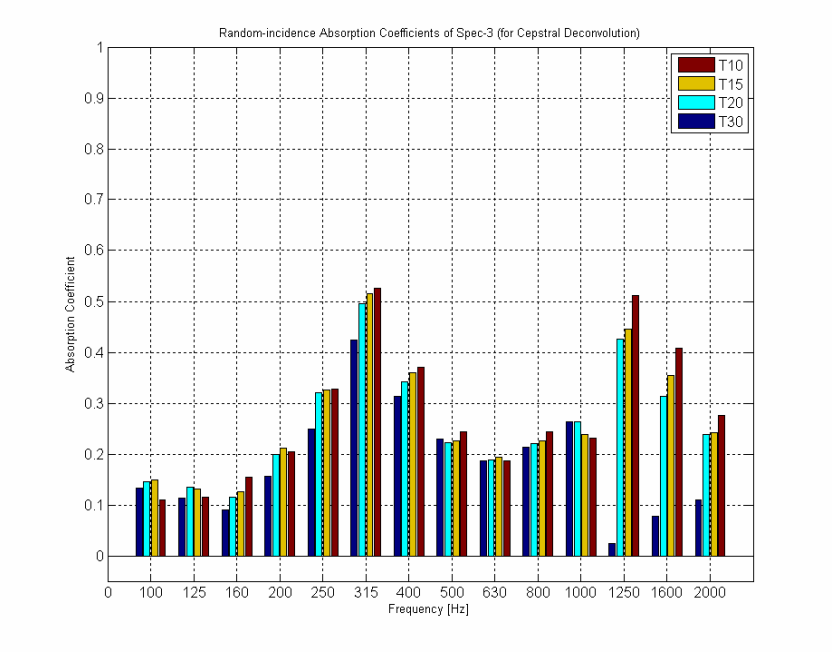

Figure 5.33 – Random-incidence absorption coefficients of specimen 3 (Cepstral Deconvolution)

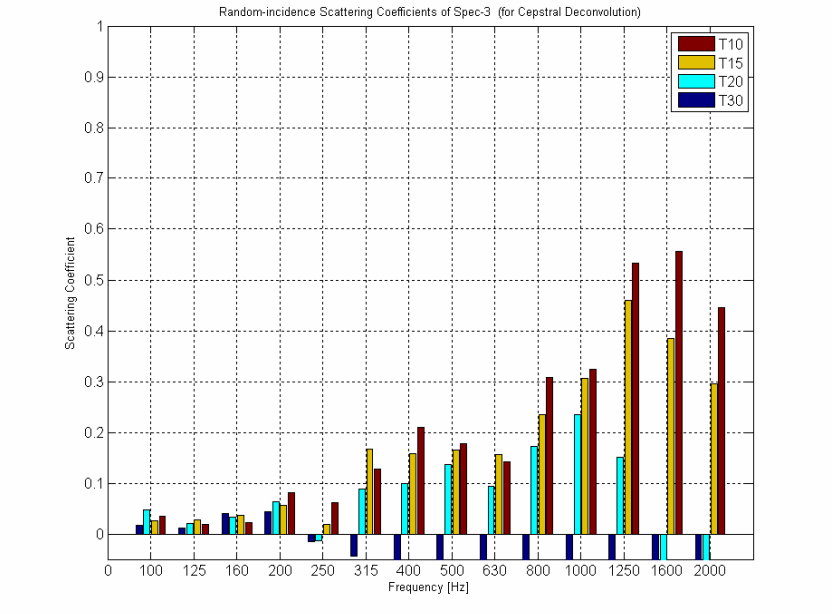

Figure 5.34 – Random-incidence scattering coefficients of specimen 3 (Cepstral Deconvolution)

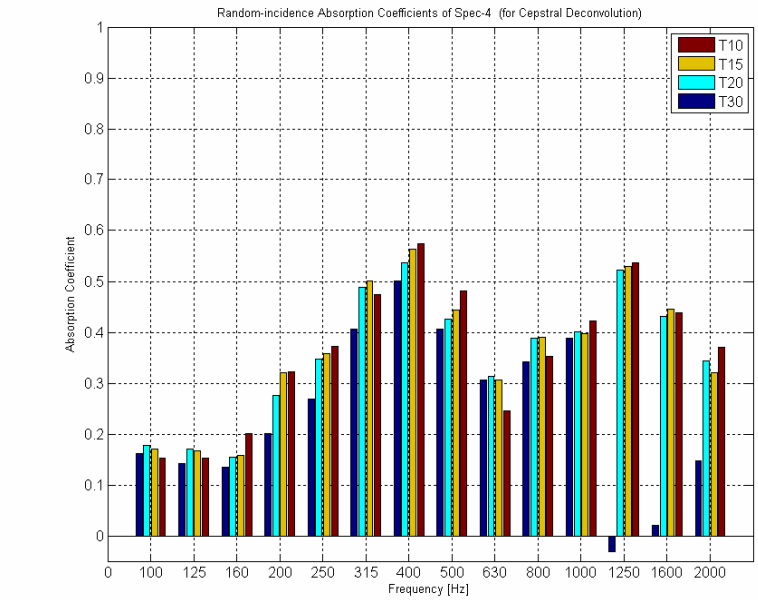

Figure 5.35 – Random-incidence absorption coefficients of specimen 4 (Cepstral Deconvolution)

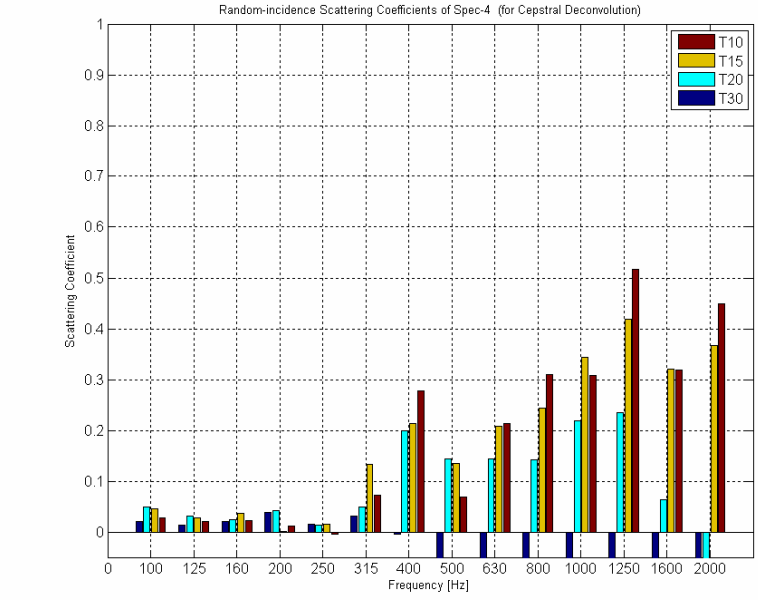

Figure 5.36 – Random-incidence scattering coefficients of specimen 4 (Cepstral Deconvolution)

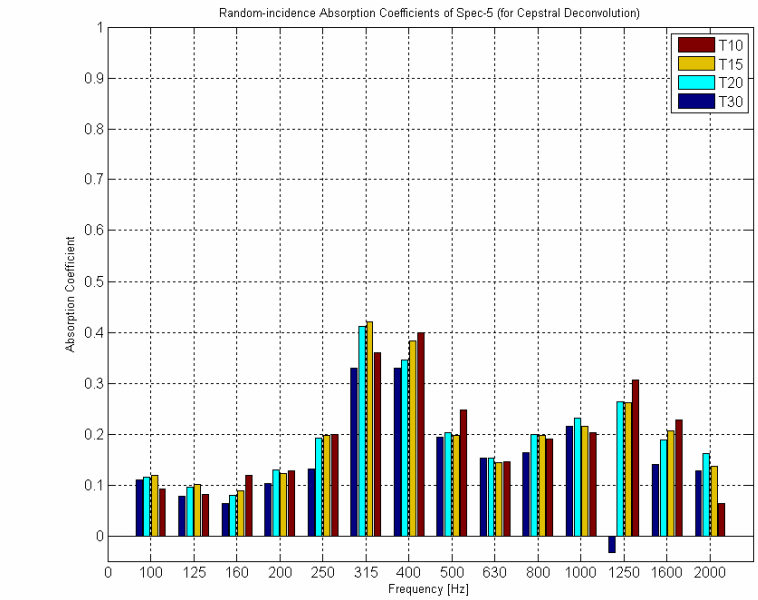

Figure 5.37 – Random-incidence absorption coefficients of specimen 5 (Cepstral Deconvolution)

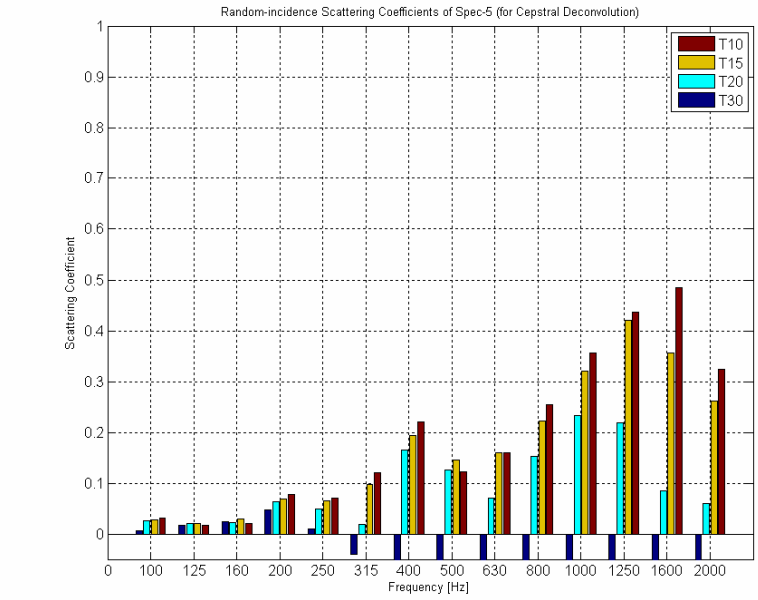

Figure 5.38 – Random-incidence scattering coefficients of specimen 5 (Cepstral Deconvolution)

5.6 Comments on Results and Discussion

5.6.1 General

All of the specimens tested are different in some crucial factors like surface detail and geometry that may influence the frequency response. The corresponding acoustical properties of these materials will also differ. However, there also exist striking similarities in their absorption and scattering behavior. For example all of the materials have very low absorption and scattering coefficients in low frequency bands with respect to the rest of the frequency bands. This behavior is expected because such properties generally increase with increasing frequency. It should also be noted that it could be rather difficult to get accurate results for frequencies below the limiting frequency (i.e. Schroeder frequency) because of the insufficient diffusion and lack of reverberant conditions as mentioned in Chapter 3.

An average value for reverberation time obtained from broadband signals (i.e. 0.6 s) can be used to make a rough estimation about the Schroeder frequency. If the corresponding values ($T = 0.6\,\text{s}$ and $V = 0.201\,\text{m}^3$) inserted into the equation 3.28, then, the limiting frequency becomes

$$f_s \approx 2000\sqrt{\frac{0.6}{0.201}} \approx 3455\ \text{Hz}$$

Since the reverberation room used is a physical scale model, value of the limiting frequency should be scaled too, i.e. for 1:10 scale reverberation room it corresponds 345.5 Hz. Moreover, this value could not be an exact value but it should be noted that below this frequency measurements would give inaccurate results.

Another similarity in these graphs is the distinguishable behavior of T_{30} curves among others at higher frequency bands. This strange behavior can be explained by combined effect of both upper limit of backward integration and frequency dependence of the decay curves. The former should be chosen carefully such that if backward integration is evaluated over a longer period, this may shorten the available evaluation range and may cause overestimated reverberation times. On the other hand if the upper limit is chosen very close to the DC value this may lead an underestimated reverberation time. Similarly, because of the frequency dependence of the decay curves, as frequency increases reverberation times can be underestimated for longer evaluation ranges i.e. 30 dB between -5 dB and -35 dB for T_{30}. These effects can be observed in Figure 5.39 and Figure 5.40 respectively.

For some of the measurements, unexpected peaks have been observed on energy decay curves (see Figure 5.40). It should be noted that these peaks may affect the straight lines constructed on evaluation ranges and result in under/overestimated reverberation times in relative frequency bands. These deviations from straight line characteristic especially at low frequency bands can be explained by echo arrival time distribution at those frequencies due to properties of enclosure and receiver and source positions as stated by Schroeder [4].

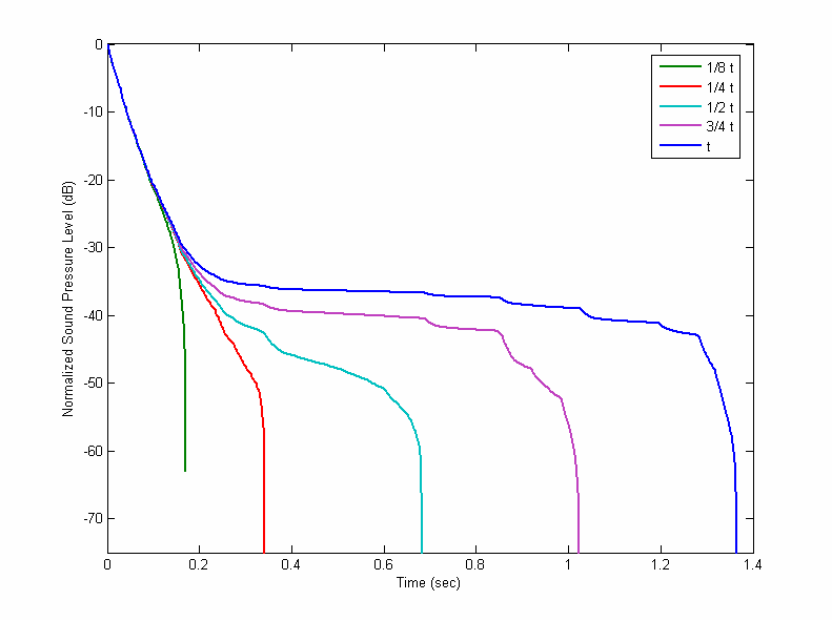

Figure 5.39 - Decay curves for various upper limit values of backward Integration (t = length of the signal)

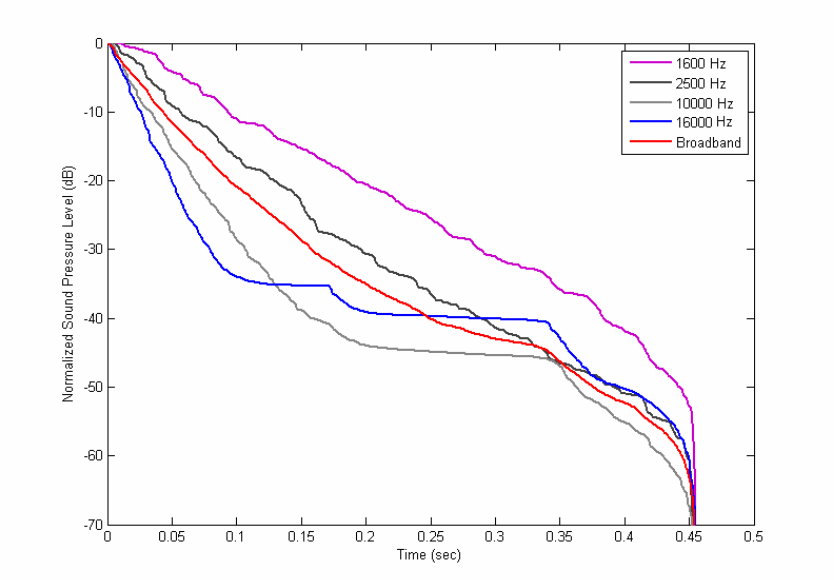

Figure 5.40 - Decay curves for different frequency bands

5.6.2 Cepstral Deconvolution

Every measurement set carried out for each reverberation time has been done for 120 impulse responses. In the application of cepstral deconvolution method, only 12 impulse responses obtained for different orientations of material/turntable and average of these 120 impulse responses have been used. The average and other 12 impulse responses are added successively. Then, total length of the signal has been completed to sample number of 1.5 million by adding zeros at the end of signal to reduce the effect of cepstral aliasing (see Figure 5.41).

Although real cepstrum for the first three reverberation time signals (T_1, T_2 and T_3) have exhibited similar characteristics in determination of peaks, the last one (T_4) has differed from them (see Figure 5.42 to Figure 5.45). This is reasonable because, orientation of the scattering surface (considering only specimen being tested and ignoring scattering from the turntable) varies only in the measurement for T_4.

The same kind of similarities and differences has been observed after liftering of the impulse responses. Particularly, differences between the first three reverberation times and the last one in deconvolved signals can be seen in Figure 5.46 and Figure 5.47.

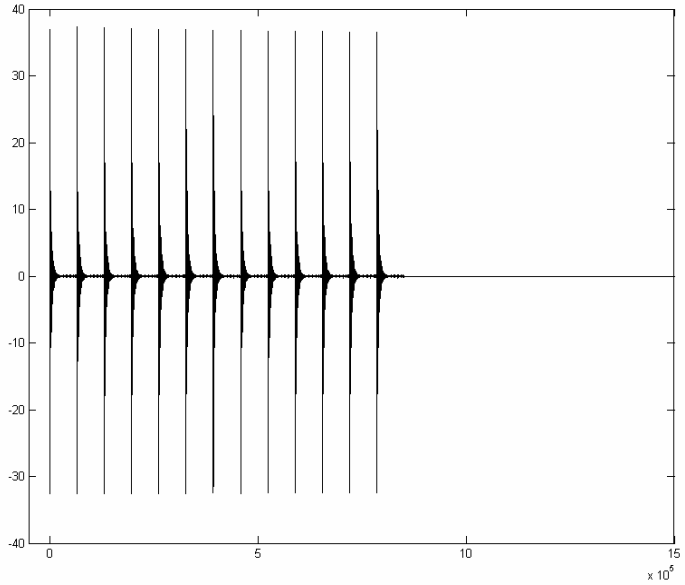

Figure 5.41 – Impulse response sequence just before cepstral deconvolution (from T_1 measurement for Specimen 2 – Mic./LS Position 1)

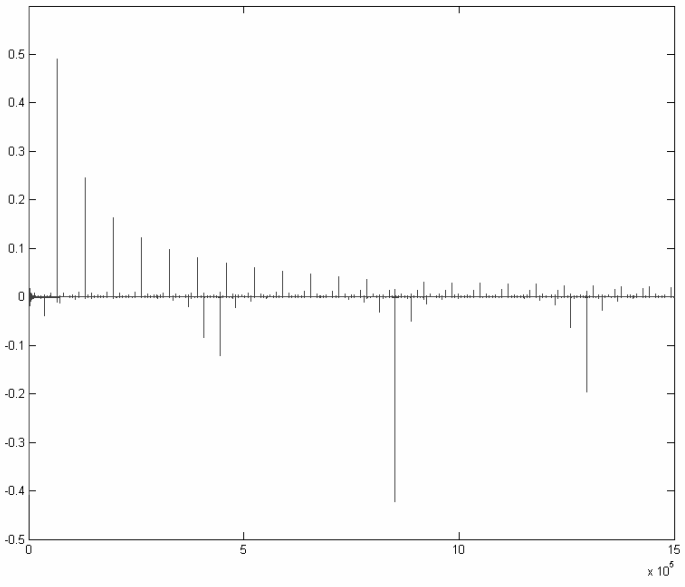

Figure 5.42 – Real cepstrum of the impulse response sequence (from T_1 measurement for Specimen 2 – Mic./L.S. Position 1)

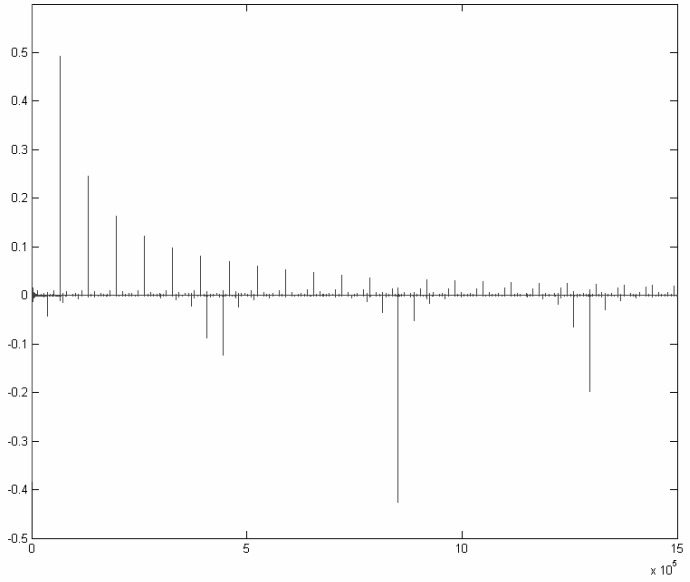

Figure 5.43 – Impulse response sequence just before cepstral deconvolution (from T_2 measurement for Specimen 2 – Mic./L.S. Position 1)

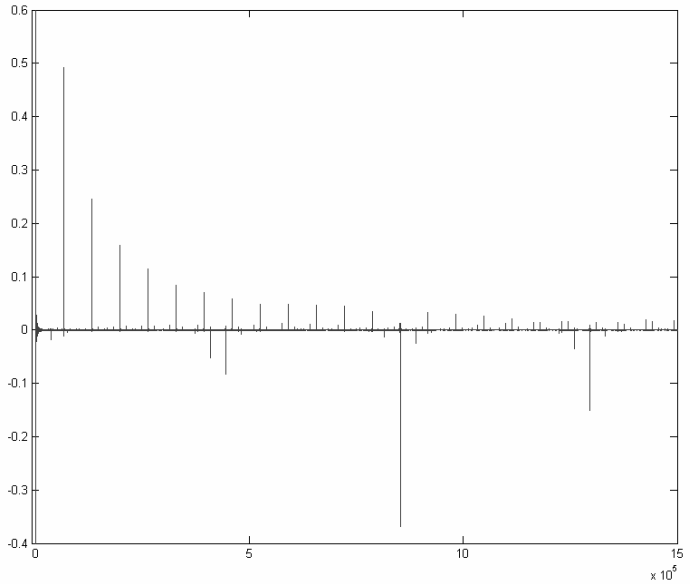

Figure 5.44 – Impulse response sequence just before cepstral deconvolution (from T_3 measurement for Specimen 2 – Mic./L.S. Position 1)

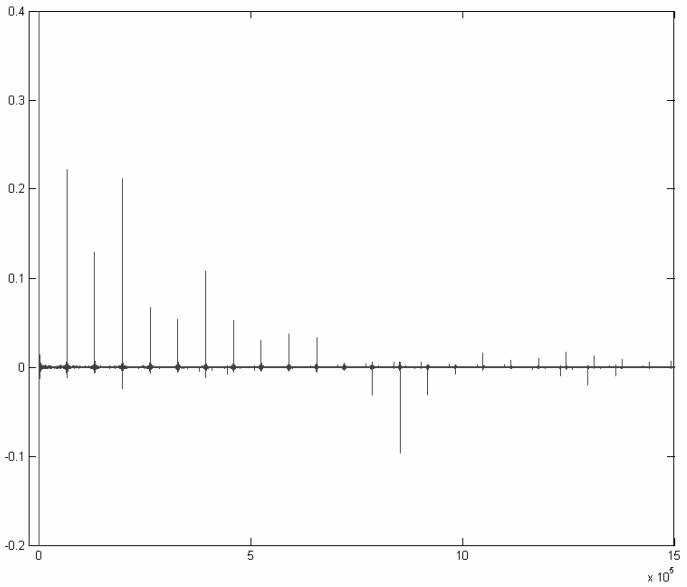

Figure 5.45 – Real cepstrum of the impulse response sequence (from T_4 measurement for Specimen 2 – Mic./L.S. Position 1)

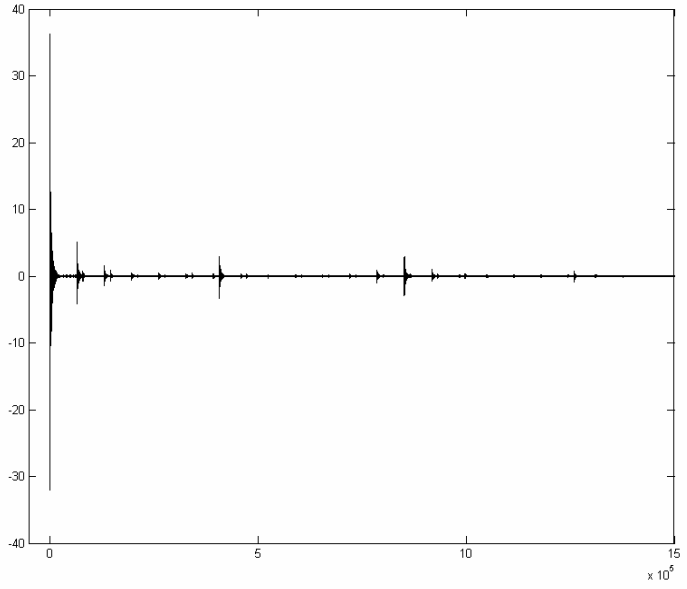

Figure 5.46 – Deconvolved impulse response sequence (from T_1 measurement for Specimen 2 – Mic./L.S. Position 1)

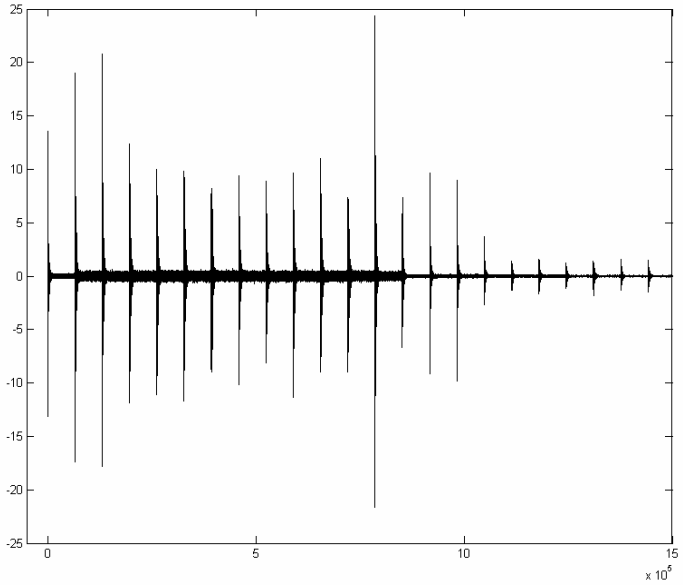

Figure 5.47 – Deconvolved impulse response sequence
(from T_4 measurement for Specimen 2 – Mic./L.S. Position 1)

In summary, the difference between two approaches, i.e. ISO method and cepstral deconvolution can be seen in graphical form of the average of the deconvolved specular impulse responses subtracted from the average of the impulse responses as shown in Figure 5.48 and Figure 5.49.

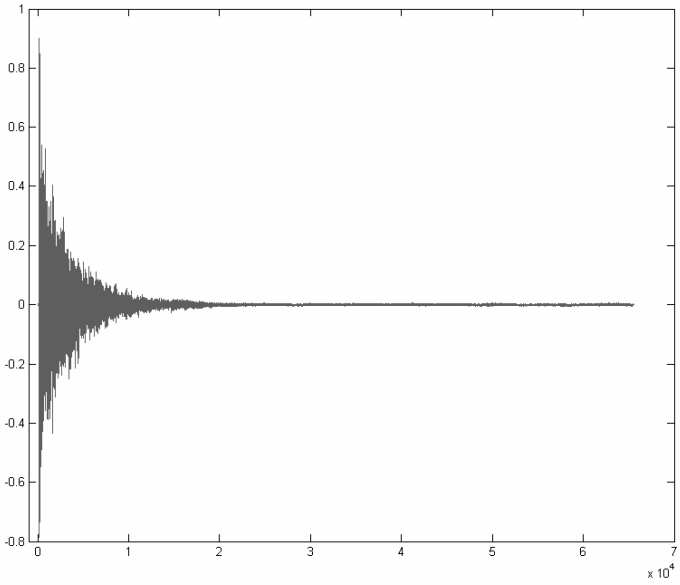

Figure 5.48 – The average of the impulse responses minus the average of the deconvolved specular impulse responses
(from T_1 measurement for Specimen 2 – Mic./L.S. Position 1)

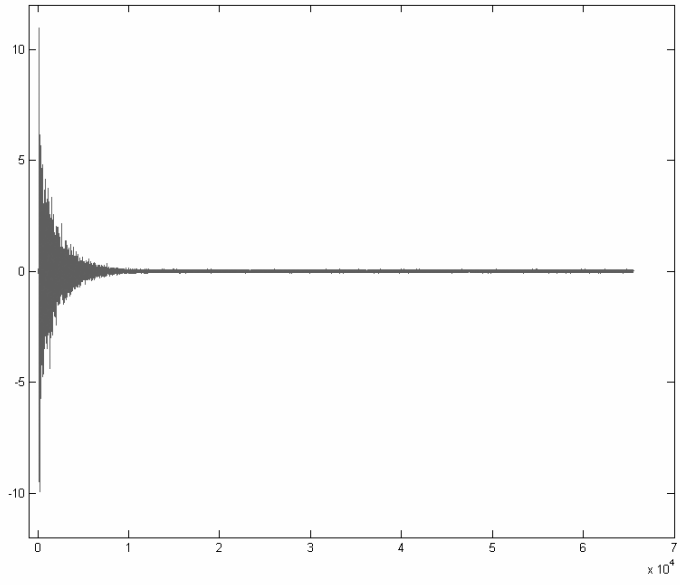

Figure 5.49 – The average of the impulse responses minus the average of the deconvolved specular impulse responses
(from T_4 measurement for Specimen 2 – Mic./L.S. Position 1)

CHAPTER 6

SUMMARY AND CONCLUSIONS

6.1 Summary

In this study, a new method for the measurement of random-incidence absorption and scattering coefficients of materials has been developed. The method is checked with a measurement technique in a reverberation room which has been standardized recently [1]. This technique, i.e. ISO method, includes measurement of impulse responses in a reverberation room and their evaluation to find random-incidence absorption and scattering coefficients for a test material. First of all, under the assumption of scattered parts of impulse responses are statistically independent, measured impulse responses are averaged. By this way, the essential part of impulse responses for calculations, i.e. their specular part, is obtained. Then, energy decay curves and reverberation times are evaluated. Finally, random-incidence absorption and scattering coefficients of the material tested are found. However, the new method proposed in this study deviates from this technique at early stages of assessment of impulse responses. Specular parts of impulse responses are separated from the rest of the impulse responses by using cepstral analysis. Cepstral analysis is known as a very powerful tool for echo detection and cancellation. The starting point of this study is the idea that, since specular parts of successive impulse responses are not changed due to orientation of tested sample throughout a measurement set, it could be possible to separate them by cepstral deconvolution. In this case echoes of a basic signal are replaced by specular parts of impulse responses. Therefore, it is anticipated that it could be possible to obtain more accurate specular parts distorted with scattered part lesser than the averaged one.

A reverberation room with a 1:10 physical scale ratio has been designed considering the restrictions specified in respective ISO standards (see Appendix A) and constructed. Its walls, floor and cover have been made of 20 mm thick Plexiglas and a turntable made of MDF and driven by a DC motor has been located in the middle of its floor. Instrumentation used consisted of two groups; equipment for sound signal production (PC, soundcard, integrated amplifier and loudspeakers) and for data acquisition (microphone, preamplifier, microphone power supply, soundcard and PC). Microphone and loudspeakers positions have been determined with respect to standards (see Appendix A).

As the excitation signal, a broadband noise signal generated from a maximum-length sequence in MATLAB is used. All of recorded and generated signals used in measurements and evaluations are sampled with a frequency of 48 kHz. Therefore, requirements of Nyquist sampling theorem have been fulfilled for frequency of interest up to about 23 kHz. In addition, because it is the default sampling rate on the soundcard used, recording and production of signals has been accomplished without any down/up sampling.

All of the random-incidence absorption and scattering coefficients are evaluated in one-third-octave bands with center frequencies of 1 kHz to 20 kHz. Broadband signals have been filtered by using one-third-octave band pass filters designed in Filter Analysis and Design Toolbox of MATLAB. In the design of these filters, Butterworth filter characteristics have been used and the requirements of the relative standard have been taken into account [20].

Evaluation of measurement results has been done by several subroutines written in MATLAB environment. These subroutines have been employed to perform all necessary tasks listed below in the following order:

1. Importing recorded sound signal to MATLAB environment,
2. Applying Fast Hadamard Transform to the signal recorded to obtain impulse responses,
3. Averaging impulse responses,
4. Performing cepstral deconvolution, just for cepstral deconvolution method,
5. Filtering impulse responses in one-third-octave bands and evaluating decay curves,
6. Employing least squares fit on decay curves and estimating reverberation times,
7. Averaging reverberation times in spatial manner,
8. Calculating environmental factors affecting air attenuation,
9. Calculating random-incidence absorption and scattering coefficients,
10. Writing results on a log file in tabular form.

Measurement procedures have been performed for five different test specimens. Then, acquired data has been evaluated with using both of the methods separately. Results obtained for these two methods have been compared for both absorption and scattering coefficients.

6.2 Conclusions

Conclusions reached upon observations are presented in two parts; comparison of results for these two methods and concluding remarks about the cepstral deconvolution method.

6.2.1 Comparison of Results for ISO Method and Cepstral Deconvolution

As shown from the results (see Appendix C), especially focusing on most reliable values of T_{10} and T_{15}, both of the methods gave almost the same results for

random-incidence absorption coefficients for all of the specimens (see Figure 6.1). This is reasonable, because, in the calculation of absorption coefficients only T_1 and T_2 values affect the results (small changes in c and m can be discarded). One should note that from both of the methods identical values have been obtained for these two reverberation times. As a matter of fact, first three reverberation times have very similar characteristics. In measurements of these T values, impulse responses have not changed significantly throughout a measurement set. Therefore, these impulse responses happen to be almost identical with their average. This causes separation of the whole signal instead of its specular part in cepstral deconvolution. In conclusion, almost the same impulse response is used in the rest of evaluations and calculations.

On the contrary, results of random-incidence scattering coefficients have exhibited strong deviations from each other for two methods especially at higher frequencies (see Figure 6.2). This is due to difference in T_4 values have been obtained for two methods. For longer evaluation ranges on decay curves the difference has become much more noticeable as shown in Figure 6.2. The interpretation of this outcome is that the sound pressure level difference between the root-mean-square amplitude of signal and background noise and so in turn signal-to-noise ratio is reduced due to the subtraction of specular part from the original impulse response performed in cepstral deconvolution method (see Figure 6.3).

All of the results obtained for random-incidence absorption and scattering coefficients calculated for all of the materials have been presented in tabular form in Appendix C.

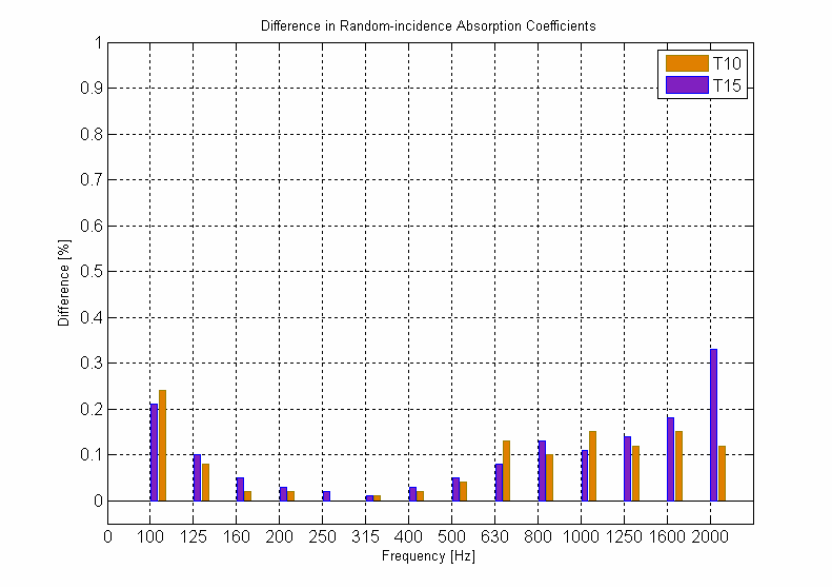

Figure 6.1 – Absolute difference between ISO Method and Cepstral Deconvolution in random-incidence absorption coefficients for specimen 2

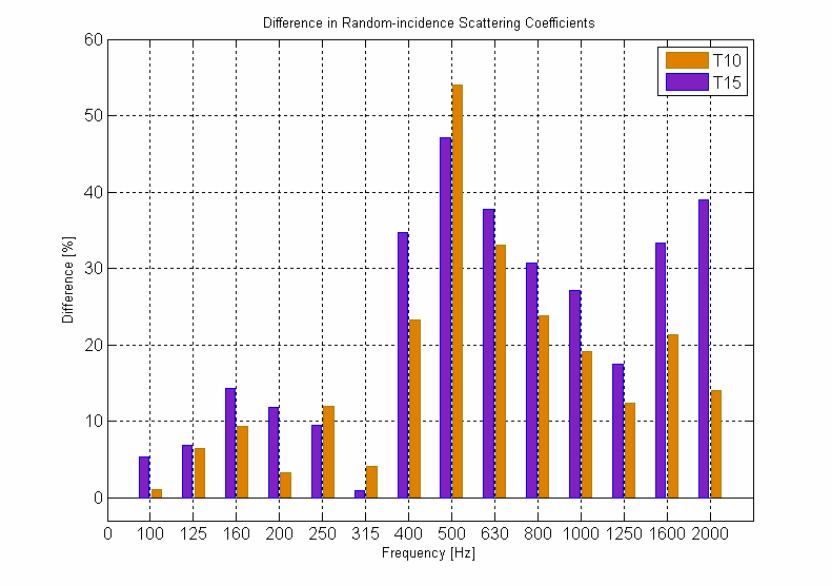

Figure 6.2 – Absolute difference between ISO Method and Cepstral Deconvolution in random-incidence scattering coefficients for specimen 2

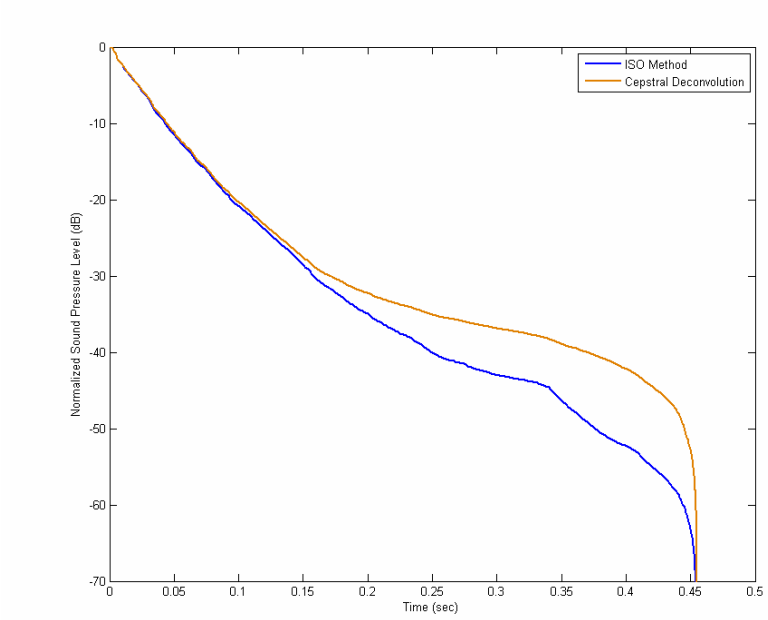

Figure 6.3 – Energy decay curves obtained by using ISO Method and Cepstral Deconvolution for broadband signal
(from T_4 measurement for Specimen 2 – Mic./L.S. Position 1)

6.2.3 Concluding Remarks on Cepstral Deconvolution Method

In this study, cepstral deconvolution has been applied on sequences consisted of 12 successive impulse responses out of 120 and their average at the beginning of this sequence. Impulse response sequences for T_1, T_2 and T_3 have been deconvolved successfully. On the other hand, deconvolved of sequences for T_4 have been suffered from some unexpected residuals with noticeable amplitudes (see Figure 5.46). Main reason of this phenomenon can be explained with cepstral aliasing and insufficient liftering. Cepstral aliasing could be reduced by adding more zeros. Nevertheless, lack of an optimum liftering algorithm makes observation and modification of all deconvolution processes as the cepstral analysis algorithm is being operated necessary.

Cepstral deconvolution method yields very close results for absorption coefficients with error levels less than 1 % in general and 3.49 % at most for reliable evaluation ranges when compared results obtained from ISO method. However, the proposed method produces scattering coefficients much lower than those measured by ISO method. In that respect these results of scattering coefficients are thought to serve as lower bounds for their corresponding values.

6.3 Future Work

Suggestions and recommendations given below could be helpful for future studies on this subject:

1. Measurements could be repeated for different type of excitation signals such as sine sweeps or maximum-length sequences of different order or tap positions.
2. Cepstral deconvolution algorithm could be refined for different numbers of impulse responses.
3. Wider frequency ranges could be swept by employing proper equipments.
4. Measurements could be performed for flush mounted or round shaped specimens to reduce the edge effect during measurements.
5. Different type of band filters could be implemented for measured data.

REFERENCES

[1] ISO 17497-1, "Acoustics – Sound-scattering properties of surfaces – Part 1: Measurement of the random-incidence scattering coefficient in a reverberation-room", International Organization for Standardization, 2004.

[2] Leo L. Beranek, István L. Vér, "Noise and Vibration Control Engineering", John Wiley and Sons, 1992.

[3] ISO 354, "Acoustics – Measurement of sound absorption in a reverberation room", International Organization for Standardization, 2003.

[4] M. R. Schroeder, "New Method of Measuring Reverberation Time", Journal of Acoustical Society of America 37, pp. 409-412, 1965.

[5] M. R. Schroeder, "Integrated-impulse method measuring sound decay without using impulses", Journal of Acoustical Society of America 66, pp. 497-500, 1979.

[6] W. T. Chu, "Impulse-Response and Reverberation-Decay Measurements Made by Using a Periodic Pseudorandom Sequence", Applied Acoustics 29, pp. 193-205, 1990.

[7] M. R. Schroeder, "Diffuse sound reflection by maximum-length sequences", Journal of Acoustical Society of America 57, pp. 149-150, 1975.

[8] Michael Vorländer, Eckard Mommertz, "Definition and measurement of random-incidence scattering coefficients", Applied Acoustics 60, pp. 187-199, 2000.

[9] Jin Yong Jeon, Sung Chan Lee, Michael Vorländer, "Development of scattering surfaces for concert halls", Applied Acoustics 65, pp. 341-355, 2004.

[10] Eckard Mommertz, “Determination of scattering coefficients from the reflection directivity of architectural surfaces”, Applied Acoustics 60, pp. 201-203, 2000.

[11] AES-4id-2001, “AES information document for room acoustics and sound reinforcement systems – Characterization and measurement of surface scattering uniformity”, Audio Engineering Society, 2001.

[12] Angelo Farina, “Measurement of the surface scattering coefficient: comparison of the Mommertz/Vorländer approach with the new Wave Field Synthesis method” International Symposium on Surface Diffusion in Room Acoustics, Liverpool, GB, 16 April 2000.

[13] Angelo Farina, “A new method for measuring the scattering coefficient and the diffusion coefficient of panels”, Acustica/Acta Acustica, vol. 86, n. 6 pp. 928-942, 2000.

[14] Heinrich Kuttruff, Room Acoustics, Spon Press, London, 4th Edition, 2000.

[15] ISO 9613-1, “Acoustics – Attenuation of sound during propagation outdoors – Part 1: Calculation of the absorption of sound by the atmosphere”, International Organization for Standardization, 1993.

[16] Donald G. Childers, David P. Skinner, Robert C. Kemerait, “The Cepstrum: A Guide to Processing”, Proceedings of the IEEE 65, pp. 1428-1443, 1977.

[17] Alan V. Oppenheim, Ronald W. Schafer, “Discrete-Time Signal Processing”, Prentice Hall, Englewood Cliffs, New Jersey, 1989.

[18] Arzu Canlı, “A New Method for the Measurement of Acoustic Properties by Cepstral Analysis”, MS Thesis, Middle East Technical University, Ankara, 1991.

[19] R. C. Kemerait, D. G. Childers, “Signal Detection and Extraction by Cepstrum Techniques”, IEEE Transactions on Information Theory IT-18, pp. 745-759, 1972.

[20] IEC 61260, “Electroacoustics – Octave-band and fractional-octave-band filters”, International Electrotechnical Commission, 1995.

APPENDIX A

REQUIREMENTS GIVEN IN ISO STANDARDS

Requirements given in the related standards for a reverberation room and instrumentation to be used and the corresponding values used in this study are listed below [1, 3]:

Table A.1 – Requirements given in the standards

Requirement	**Standard**	**Used (N=10)**
The volume of the room (V) [m^3]	$\geq 200 \times N^{-3}$ (= 0.2)	0.201
The equivalent absorption area of the empty room (A_1) [m^2]	$\leq 0.30 \times V^{2/3}$ (= 0.103)	0.058 (max.)
Distance between turntable and room walls [m]	$\geq N^{-1} \times 1.0$ (= 0.1)	0.11
Diameter for base plate-square sample (d) [m]	$\geq N^{-1} \times 3.75$ (= 0.375)	0.38
Structural depth of the sample (h) [m]	$\leq d/16$ (= 0.024)	0.02 (max.)
Longest straight line within the room (I_{max}) [m]	$< 1.9 \times V^{1/3}$ (= 1.113)	1.046
Distance between microphone positions [m]	$> 1.5 \times N^{-1}$ (= 0.15)	0.16 (min.)
Distance between microphone and source positions [m]	$> 2.0 \times N^{-1}$ (= 0.2)	0.45 (min.)
Distance between microphone positions and room walls [m]	$> 1.0 \times N^{-1}$ (= 0.1)	0.11 (min.)
Distance between sound sources positions [m]	$> 3.0 \times N^{-1}$ (= 0.3)	0.5

Table A.2 – Maximum scattering coefficient of the base plate s_{base}

Frequency (*f*/*N*) [Hz]	**100**	**125**	**160**	**200**	**250**	**315**	**400**
Standard	0.05	0.05	0.05	0.05	0.05	0.05	0.05
Used	0.002	0.002	0.001	0.002	0.001	0.001	0.001

Frequency (*f*/*N*) [Hz]	**500**	**630**	**800**	**1000**	**1250**	**1600**	**2000**
Standard	0.05	0.10	0.10	0.10	0.15	0.15	0.15
Used	0.003	0.004	0.003	0.007	0.008	0.016	0.015

APPENDIX B

MLS GENERATION AND FAST HADAMARD TRANSFORM

B.1 Generation of a Maximum-Length Sequence

A maximum-length sequence is generated by employing a modulo-2 arithmetic (or exclusive-OR, XOR) operation embedded in a shift register in which number of steps is equal to the degree of the sequence to be generated. The scheme of the modulo-2 arithmetic operation ($\oplus$) is shown below

$$1 \oplus 0 = 0 \oplus 1 = 1$$
$$0 \oplus 0 = 1 \oplus 1 = 0$$

The modulo-2 arithmetic operation is performed between the first and the last elements of the current number set of length n. The output of the operation is fed back to the input and this is repeated for ($2^n - 1$) times until the sequence is completed. Let the order of the MLS be 3 (i.e. $n = 3$) and the operation is begun with set of ones (1 0 0)

As it is shown in Table B.1 the current number set on the second column is repeating with a period of seven steps so the sequence generated. Therefore the sequence generated on seventh step (1 1 0 1 0 0 1) gives the MLS after the elements of this sequence is converted to +1 and -1 instead of 0 and 1 such that (-1 -1 1 -1 1 1 -1).

Table B.1- Modulo-2 arithmetic operation

Step No	Current Number Set	Result of Modulo-2 Operation	Sequence Generated
1	1 0 0	1	1
2	1 1 0	1	1 1
3	1 1 1	0	1 1 0
4	0 1 1	1	1 1 0 1
5	1 0 1	0	1 1 0 1 0
6	0 1 0	0	1 1 0 1 0 0
7	0 0 1	1	1 1 0 1 0 0 1
8	1 0 0	1	1 1 0 1 0 0 1 1

B.2 Fast Hadamard Transformation

The procedure described below is based on the method specified by Chu [6].

Let the maximum-length sequence used in a measurement be the one generated above such that

$$s_k = \begin{bmatrix} s_1 \\ s_2 \\ s_3 \\ s_4 \\ s_5 \\ s_6 \\ s_7 \end{bmatrix} = \begin{bmatrix} -1 \\ -1 \\ +1 \\ -1 \\ +1 \\ +1 \\ -1 \end{bmatrix}$$

then the S matrix becomes

$$[S]=\begin{bmatrix} -1 & -1 & +1 & -1 & +1 & +1 & -1 \\ -1 & -1 & -1 & +1 & -1 & +1 & +1 \\ +1 & -1 & -1 & -1 & +1 & -1 & +1 \\ +1 & +1 & -1 & -1 & -1 & +1 & -1 \\ -1 & +1 & +1 & -1 & -1 & -1 & +1 \\ +1 & -1 & +1 & +1 & -1 & -1 & -1 \\ -1 & +1 & -1 & +1 & +1 & -1 & -1 \end{bmatrix}$$

Afterwards, the elements of [S] are changed with zeros (for +1s) and ones (for -1s) and also the column and the row matrices, [C] and [R] respectively are constructed

$$[S]=\begin{bmatrix} 1 & 1 & 0 & 1 & 0 & 0 & 1 \\ 1 & 1 & 1 & 0 & 1 & 0 & 0 \\ 0 & 1 & 1 & 1 & 0 & 1 & 0 \\ 0 & 0 & 1 & 1 & 1 & 0 & 1 \\ 1 & 0 & 0 & 1 & 1 & 1 & 0 \\ 0 & 1 & 0 & 0 & 1 & 1 & 1 \\ 1 & 0 & 1 & 0 & 0 & 1 & 1 \end{bmatrix} = [R]\cdot[C]$$

$$[R]=\begin{bmatrix} 1 & 0 & 0 \\ 0 & 1 & 0 \\ 0 & 0 & 1 \\ 1 & 1 & 0 \\ 0 & 1 & 1 \\ 1 & 1 & 1 \\ 1 & 0 & 1 \end{bmatrix} \underbrace{\begin{pmatrix} 4 \\ 2 \\ 1 \\ 6 \\ 3 \\ 7 \\ 5 \end{pmatrix}}_{\text{Tags for } [R]}$$

$$[C]=\begin{bmatrix} 1 & 1 & 0 & 1 & 0 & 0 & 1 \\ 1 & 1 & 1 & 0 & 1 & 0 & 0 \\ 0 & 1 & 1 & 1 & 0 & 1 & 0 \end{bmatrix}$$

$$\underbrace{\begin{pmatrix} 6 & 7 & 3 & 5 & 2 & 1 & 4 \end{pmatrix}}_{\text{Tags for } [C]}$$

Next the columns of the matrix [S] is rearranged according to the tags for [C] such that the 6th column of the [S] (tagged as 1st) moved to 1st column position

and it is repeated for all seven columns of [*S*] to form the matrix [*S*]'. Then the rows of [*S*]' are reordered similarly such as the 5th row of the [*S*]' (tagged as 3rd) is shifted to 3rd row and this process repeated again seven times and the matrix [*S*]" is obtained.

$$[S]' = \begin{bmatrix} 0 & 0 & 0 & 1 & 1 & 1 & 1 \\ 0 & 1 & 1 & 0 & 0 & 1 & 1 \\ 1 & 0 & 1 & 0 & 1 & 0 & 1 \\ 0 & 1 & 1 & 1 & 1 & 0 & 0 \\ 1 & 1 & 0 & 0 & 1 & 1 & 0 \\ 1 & 1 & 0 & 1 & 0 & 0 & 1 \\ 1 & 0 & 1 & 1 & 0 & 1 & 0 \end{bmatrix} \qquad [S]'' = \begin{bmatrix} 1 & 0 & 1 & 0 & 1 & 0 & 1 \\ 0 & 1 & 1 & 0 & 0 & 1 & 1 \\ 1 & 1 & 0 & 0 & 1 & 1 & 0 \\ 0 & 0 & 0 & 1 & 1 & 1 & 1 \\ 1 & 0 & 1 & 1 & 0 & 1 & 0 \\ 0 & 1 & 1 & 1 & 1 & 0 & 0 \\ 1 & 1 & 0 & 1 & 0 & 0 & 1 \end{bmatrix}$$

Finally all the elements of [*S*]" are converted to +1s and -1s following the same procedure as done above reversely and a row and a column of +1s are added to form [*S*]"' as an Hadamard matrix of order 3. For only the signs of the elements

$$[H_3] = [S]''' = \begin{bmatrix} + & + & + & + & + & + & + & + \\ + & - & + & - & + & - & + & - \\ + & + & - & - & + & + & - & - \\ + & - & - & + & + & - & - & + \\ + & + & + & + & - & - & - & - \\ + & - & + & - & - & + & - & + \\ + & + & - & - & - & - & + & + \\ + & - & - & + & - & + & + & - \end{bmatrix}$$

Let s' be the output signal recorded for one period of the MLS signal considered above. First it is rearranged with respect to the tags for [*C*] matrix then a zero element added to this modified output matrix [*S'*]'

$$[S'] = \begin{bmatrix} s'_1 \\ s'_2 \\ s'_3 \\ s'_4 \\ s'_5 \\ s'_6 \\ s'_7 \end{bmatrix}, \quad [S']' = \begin{bmatrix} s'_6 \\ s'_5 \\ s'_3 \\ s'_7 \\ s'_4 \\ s'_1 \\ s'_2 \end{bmatrix}, \quad [S']'' = \begin{bmatrix} 0 \\ s'_6 \\ s'_5 \\ s'_3 \\ s'_7 \\ s'_4 \\ s'_1 \\ s'_2 \end{bmatrix}$$

Then the modified impulse response [*h*]" is obtained by

$$[h]'' = \underbrace{\begin{bmatrix} + & + & + & + & + & + & + & + \\ + & - & + & - & + & - & + & - \\ + & + & - & - & + & + & - & - \\ + & - & - & + & + & - & - & + \\ + & + & + & + & - & - & - & - \\ + & - & + & - & - & + & - & + \\ + & + & - & - & - & - & + & + \\ + & - & - & + & - & + & + & - \end{bmatrix}}_{[H_3]\left(=[S]'''\right)} \cdot \underbrace{\begin{bmatrix} 0 \\ s'_6 \\ s'_5 \\ s'_3 \\ s'_7 \\ s'_4 \\ s'_1 \\ s'_2 \end{bmatrix}}_{[S']''}$$

The matrix multiplication above is done by using butterfly algorithm of n steps (numbers represent the corresponding elements of the output signal except 0).

Finally first element of the [*h*]" is removed and the remaining elements are reordered according to the tags of [*R*] in order to obtain the impulse response [*h*].

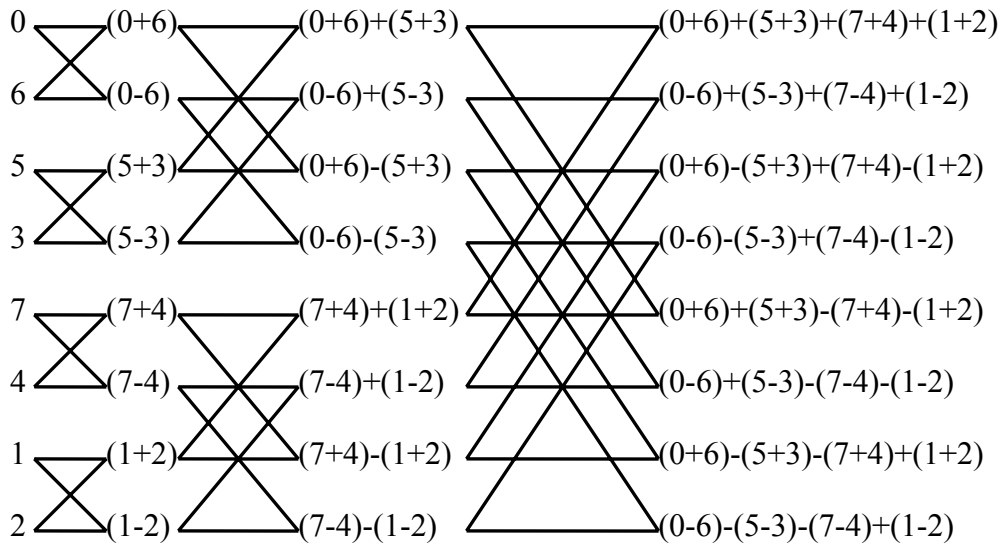

Figure B.1 – Fast Hadamard transform butterfly algorithm scheme

APPENDIX C

MEASUREMENT RESULTS

Calculated random-incidence absorption and scattering coefficients for all of five specimens given in Table C.1. Results for both of the methods are presented in one-third-octave bands and for four different reverberation time evaluation ranges.

Table C.1 – Random-incidence absorption and scattering coefficients of the specimens calculated according to both methods

Specimen-1

Random-Incidence Absorption Coefficients for ISO Method

f (Hz)	100	125	160	200	250	315	400	500	630	800	1000	1250	1600	2000
T_{10}	0,080	0,067	0,113	0,078	0,138	0,166	0,153	0,210	0,245	0,249	0,278	0,374	0,321	0,431
T_{20}	0,119	0,082	0,069	0,074	0,099	0,132	0,157	0,188	0,215	0,264	0,265	0,349	0,364	0,347
T_{30}	0,107	0,063	0,052	0,056	0,070	0,120	0,132	0,176	0,206	0,247	0,280	0,321	0,132	0,094
T_{15}	0,110	0,080	0,070	0,071	0,124	0,143	0,156	0,182	0,235	0,251	0,259	0,378	0,387	0,323

Random-Incidence Absorption Coefficients for Cepstral Deconvolution Method

T_{10}	0,080	0,067	0,113	0,078	0,138	0,167	0,153	0,210	0,245	0,249	0,278	0,374	0,321	0,431
T_{20}	0,118	0,082	0,069	0,074	0,099	0,132	0,157	0,188	0,215	0,264	0,266	0,349	0,364	0,347
T_{30}	0,107	0,063	0,052	0,056	0,070	0,120	0,133	0,176	0,206	0,246	0,280	0,319	0,130	0,096
T_{15}	0,110	0,080	0,070	0,072	0,124	0,143	0,156	0,182	0,235	0,251	0,259	0,378	0,387	0,323

Random-Incidence Scattering Coefficients for ISO Method

T_{10}	0,054	0,018	0,061	0,078	0,025	0,141	0,183	0,230	0,245	0,273	0,379	0,327	0,498	0,536
T_{20}	0,027	0,026	0,058	0,070	0,090	0,113	0,162	0,230	0,315	0,326	0,326	0,394	0,452	0,473
T_{30}	0,015	0,023	0,050	0,074	0,054	0,081	0,137	0,198	0,260	0,310	0,290	0,343	0,005	-0,008
T_{15}	0,042	0,031	0,072	0,058	0,062	0,141	0,167	0,256	0,298	0,318	0,346	0,416	0,464	0,461

Random-Incidence Scattering Coefficients for Cepstral Deconvolution Method

T_{10}	0,053	0,017	0,058	0,079	0,001	0,117	0,143	0,178	0,243	0,195	0,339	0,286	0,419	0,410
T_{20}	0,026	0,024	0,056	0,071	0,083	0,090	0,096	0,138	0,217	0,248	0,239	0,315	0,305	0,321
T_{30}	0,010	0,020	0,045	0,066	0,046	0,030	0,010	-0,011	-0,072	-0,114	-0,156	-0,630	-0,667	-0,420
T_{15}	0,041	0,029	0,071	0,062	0,048	0,119	0,118	0,183	0,235	0,263	0,274	0,355	0,350	0,346

Specimen-2

Random-Incidence Absorption Coefficients for ISO Method

f (Hz)	100	125	160	200	250	315	400	500	630	800	1000	1250	1600	2000
T10	0,118	0,124	0,166	0,246	0,322	0,484	0,459	0,345	0,223	0,273	0,336	0,484	0,447	0,334
T20	0,143	0,144	0,132	0,211	0,316	0,487	0,440	0,304	0,236	0,241	0,337	0,463	0,384	0,315
T30	0,139	0,127	0,109	0,173	0,243	0,402	0,431	0,297	0,235	0,240	0,327	0,107	0,092	0,189
T15	0,143	0,141	0,133	0,229	0,328	0,506	0,446	0,308	0,246	0,241	0,343	0,454	0,398	0,296

Random-Incidence Absorption Coefficients for Cepstral Deconvolution Method

T10	0,118	0,124	0,166	0,246	0,322	0,485	0,459	0,346	0,223	0,273	0,336	0,485	0,448	0,334
T20	0,144	0,145	0,132	0,211	0,316	0,487	0,440	0,304	0,236	0,241	0,338	0,464	0,385	0,316
T30	0,139	0,127	0,108	0,173	0,243	0,401	0,431	0,297	0,236	0,240	0,327	0,095	0,086	0,189
T15	0,143	0,141	0,133	0,229	0,328	0,506	0,447	0,308	0,246	0,241	0,344	0,455	0,399	0,297

Random-Incidence Scattering Coefficients for ISO Method

T10	0,047	0,019	0,026	0,043	0,042	0,111	0,328	0,186	0,173	0,314	0,308	0,778	0,769	0,554
T20	0,073	0,029	0,018	0,059	0,003	0,082	0,259	0,233	0,242	0,289	0,299	0,578	0,571	0,554
T30	0,047	0,020	0,012	0,049	0,025	0,074	0,161	0,201	0,235	0,275	0,324	0,039	-0,009	-0,057
T15	0,050	0,032	0,030	0,055	0,011	0,142	0,276	0,228	0,240	0,313	0,293	0,690	0,653	0,632

Random-Incidence Scattering Coefficients for Cepstral Deconvolution Method

T10	0,046	0,018	0,029	0,042	0,047	0,106	0,252	0,086	0,116	0,239	0,249	0,682	0,605	0,477
T20	0,069	0,027	0,021	0,053	0,000	0,082	0,138	0,113	0,140	0,177	0,202	0,316	0,069	-0,040
T30	0,050	0,016	0,012	0,039	0,008	0,050	-0,167	-0,203	-0,339	-0,462	-0,730	-0,508	-0,732	-0,555
T15	0,047	0,030	0,035	0,049	0,010	0,141	0,180	0,121	0,149	0,217	0,214	0,570	0,435	0,386

Specimen-3

Random-Incidence Absorption Coefficients for ISO Method

f (Hz)	100	125	160	200	250	315	400	500	630	800	1000	1250	1600	2000
T10	0,110	0,115	0,154	0,205	0,328	0,525	0,370	0,243	0,187	0,244	0,231	0,512	0,407	0,277
T20	0,146	0,134	0,116	0,200	0,320	0,496	0,341	0,222	0,189	0,221	0,264	0,427	0,313	0,238
T30	0,133	0,114	0,092	0,156	0,250	0,424	0,314	0,230	0,187	0,214	0,263	0,024	0,074	0,115
T15	0,149	0,131	0,126	0,211	0,327	0,515	0,360	0,226	0,194	0,226	0,238	0,446	0,354	0,243

Random-Incidence Absorption Coefficients for Cepstral Deconvolution Method

T10	0,111	0,115	0,154	0,205	0,328	0,526	0,370	0,243	0,187	0,244	0,231	0,512	0,408	0,277
T20	0,146	0,134	0,115	0,200	0,320	0,496	0,341	0,222	0,189	0,221	0,264	0,427	0,313	0,238
T30	0,133	0,114	0,090	0,155	0,250	0,423	0,314	0,230	0,187	0,214	0,263	0,024	0,078	0,110
T15	0,150	0,131	0,126	0,211	0,327	0,515	0,360	0,226	0,194	0,226	0,238	0,446	0,354	0,243

Random-Incidence Scattering Coefficients for ISO Method

T10	0,039	0,017	0,023	0,084	0,056	0,119	0,294	0,263	0,219	0,340	0,398	0,756	0,765	0,564
T20	0,054	0,022	0,029	0,063	-0,010	0,122	0,232	0,272	0,272	0,302	0,352	0,625	0,668	0,586
T30	0,029	0,017	0,031	0,050	0,006	0,062	0,185	0,219	0,258	0,284	0,313	-0,058	-0,069	-0,046
T15	0,029	0,029	0,038	0,059	0,022	0,182	0,259	0,271	0,289	0,344	0,381	0,697	0,746	0,659

Random-Incidence Scattering Coefficients for Cepstral Deconvolution Method

T10	0,035	0,019	0,023	0,082	0,062	0,128	0,210	0,178	0,142	0,308	0,324	0,533	0,556	0,446
T20	0,048	0,021	0,032	0,063	-0,013	0,089	0,100	0,137	0,094	0,172	0,235	0,151	-0,565	-1,125
T30	0,016	0,012	0,041	0,044	-0,015	-0,044	-0,192	-0,290	-0,394	-0,540	-0,827	-0,406	-0,632	-0,410
T15	0,026	0,029	0,037	0,057	0,019	0,168	0,157	0,165	0,155	0,235	0,306	0,460	0,385	0,296

Specimen-4

Random-Incidence Absorption Coefficients for ISO Method

f (Hz)	100	125	160	200	250	315	400	500	630	800	1000	1250	1600	2000
T10	0,152	0,152	0,201	0,322	0,372	0,474	0,573	0,480	0,243	0,351	0,420	0,534	0,434	0,366
T20	0,178	0,171	0,154	0,275	0,347	0,488	0,535	0,425	0,312	0,386	0,399	0,520	0,428	0,340
T30	0,162	0,141	0,136	0,201	0,269	0,406	0,501	0,405	0,306	0,340	0,386	-0,023	0,022	0,152
T15	0,170	0,167	0,157	0,321	0,357	0,500	0,563	0,442	0,306	0,388	0,395	0,526	0,442	0,316

Random-Incidence Absorption Coefficients for Cepstral Deconvolution Method

T10	0,152	0,152	0,201	0,322	0,372	0,474	0,574	0,481	0,245	0,353	0,422	0,536	0,439	0,370
T20	0,178	0,171	0,154	0,275	0,348	0,489	0,536	0,426	0,313	0,388	0,401	0,522	0,432	0,344
T30	0,162	0,141	0,135	0,200	0,268	0,406	0,501	0,406	0,307	0,341	0,388	-0,031	0,021	0,148
T15	0,170	0,167	0,157	0,321	0,358	0,501	0,563	0,443	0,307	0,390	0,397	0,529	0,446	0,321

Random-Incidence Scattering Coefficients for ISO Method

T10	0,028	0,020	0,021	0,016	0,003	0,081	0,270	0,105	0,298	0,428	0,444	0,658	0,495	0,598
T20	0,050	0,032	0,026	0,047	0,023	0,072	0,221	0,237	0,304	0,388	0,415	0,557	0,563	0,577
T30	0,038	0,020	0,016	0,055	0,032	0,079	0,110	0,211	0,281	0,375	0,367	0,036	0,003	-0,051
T15	0,045	0,027	0,035	0,010	0,017	0,148	0,224	0,218	0,304	0,416	0,464	0,603	0,548	0,647

Random-Incidence Scattering Coefficients for Cepstral Deconvolution Method

T10	0,027	0,020	0,022	0,012	-0,004	0,073	0,277	0,068	0,214	0,310	0,309	0,516	0,318	0,450
T20	0,049	0,031	0,025	0,042	0,013	0,049	0,200	0,145	0,143	0,141	0,219	0,235	0,064	-0,358
T30	0,021	0,013	0,020	0,039	0,015	0,031	-0,004	-0,189	-0,639	-0,899	-1,258	-0,280	-0,476	-0,451
T15	0,046	0,027	0,037	0,001	0,015	0,133	0,213	0,134	0,208	0,245	0,343	0,419	0,320	0,367

Specimen-5

Random-Incidence Absorption Coefficients for ISO Method

f (Hz)	100	125	160	200	250	315	400	500	630	800	1000	1250	1600	2000
T10	0,093	0,081	0,119	0,128	0,199	0,359	0,400	0,247	0,144	0,190	0,201	0,305	0,227	0,061
T20	0,114	0,095	0,080	0,129	0,191	0,411	0,345	0,203	0,153	0,198	0,229	0,261	0,186	0,159
T30	0,109	0,078	0,064	0,104	0,131	0,331	0,329	0,194	0,152	0,163	0,215	-0,033	0,142	0,129
T15	0,118	0,100	0,088	0,122	0,197	0,420	0,383	0,197	0,144	0,197	0,214	0,261	0,204	0,135

Random-Incidence Absorption Coefficients for Cepstral Deconvolution Method

T10	0,093	0,082	0,119	0,128	0,199	0,360	0,400	0,248	0,145	0,191	0,202	0,306	0,228	0,063
T20	0,114	0,095	0,080	0,129	0,192	0,411	0,345	0,203	0,154	0,198	0,231	0,263	0,188	0,161
T30	0,109	0,077	0,064	0,103	0,131	0,330	0,329	0,194	0,153	0,163	0,216	-0,033	0,141	0,128
T15	0,118	0,100	0,088	0,122	0,197	0,421	0,384	0,198	0,145	0,198	0,215	0,262	0,206	0,137

Random-Incidence Scattering Coefficients for ISO Method

T10	0,033	0,017	0,023	0,077	0,072	0,151	0,295	0,223	0,246	0,358	0,433	0,648	0,626	0,419
T20	0,036	0,022	0,025	0,065	0,062	0,070	0,251	0,264	0,251	0,297	0,400	0,548	0,495	0,420
T30	0,003	0,014	0,020	0,053	0,036	0,050	0,182	0,227	0,225	0,286	0,355	-0,045	0,024	0,037
T15	0,031	0,024	0,037	0,068	0,071	0,144	0,260	0,270	0,292	0,338	0,417	0,615	0,533	0,428

Random-Incidence Scattering Coefficients for Cepstral Deconvolution Method

T10	0,031	0,017	0,020	0,078	0,070	0,120	0,220	0,122	0,160	0,254	0,356	0,437	0,484	0,325
T20	0,026	0,021	0,023	0,063	0,049	0,018	0,165	0,126	0,070	0,153	0,233	0,219	0,086	0,060
T30	0,006	0,016	0,024	0,048	0,010	-0,040	-0,066	-0,225	-0,362	-0,459	-0,777	-0,255	-0,586	-0,374
T15	0,028	0,021	0,030	0,068	0,065	0,098	0,194	0,145	0,159	0,222	0,321	0,421	0,356	0,262

APPENDIX D

FLUSH MOUNTING AND ACCURACY

Additional measurements have been conducted using the same setup with flush mounted test specimen (specimen 2). Standard deviations of these results have been also evaluated according to formula given in ISO 17497-1 [1].

Standard deviation of the coefficients:

$$\delta_{\alpha_s} = \frac{55.3V}{cS}\sqrt{\left(\frac{\delta_2}{T_2^2}\right)^2 + \left(\frac{\delta_1}{T_1^2}\right)^2} \tag{D.1}$$

$$\delta_{\alpha_{spec}} = \frac{55.3V}{cS}\sqrt{\left(\frac{\delta_4}{T_4^2}\right)^2 + \left(\frac{\delta_3}{T_3^2}\right)^2} \tag{D.2}$$

$$\delta_s = \left|\frac{\alpha_{spec}-1}{1-\alpha_s}\right|\sqrt{\left(\frac{\delta_{\alpha_{spec}}}{\alpha_{spec}-1}\right)^2 + \left(\frac{\delta_{\alpha_s}}{1-\alpha_s}\right)^2} \tag{D.3}$$

Where

$$\delta = \sqrt{\sum_{i=1}^{N}\frac{(T_i-\overline{T})^2}{N(N-1)}} \text{ and } \overline{T} = \frac{1}{N}\sum_{i=1}^{N}T_i$$

Here, N is the number of measurements in spatial manner and $\overline{T}$ stands for the average value of the corresponding reverberation time.

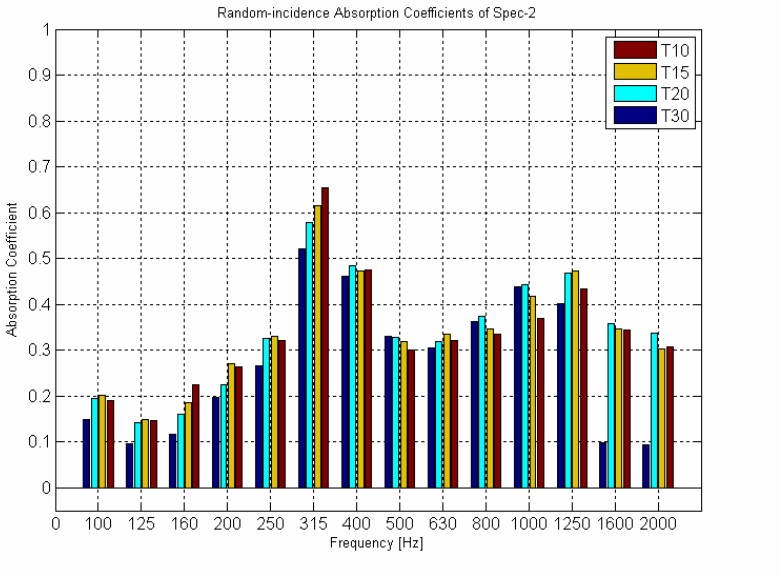

Figure D.1 – Random-incidence absorption coefficients of specimen 2 (Flush Mounting and ISO Method)

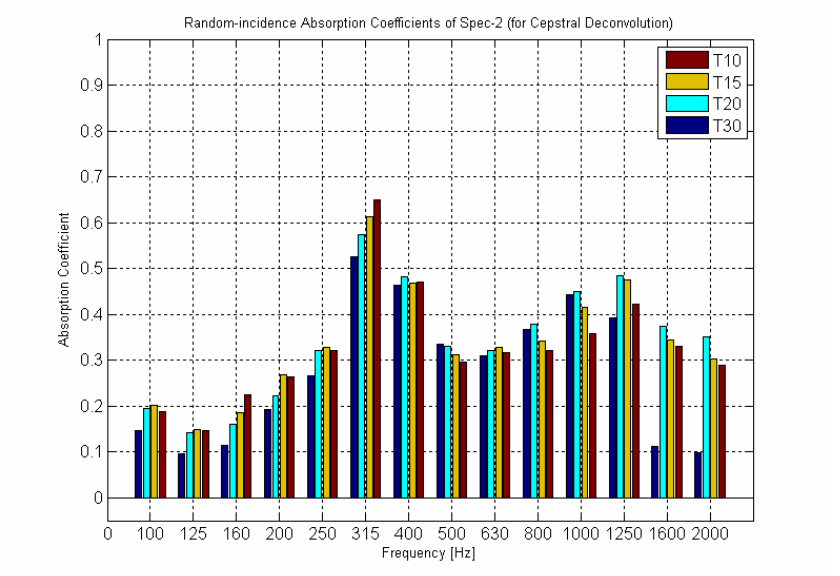

Figure D.2 – Random-incidence absorption coefficients of specimen 2 (Flush Mounting and Cepstral Deconvolution)

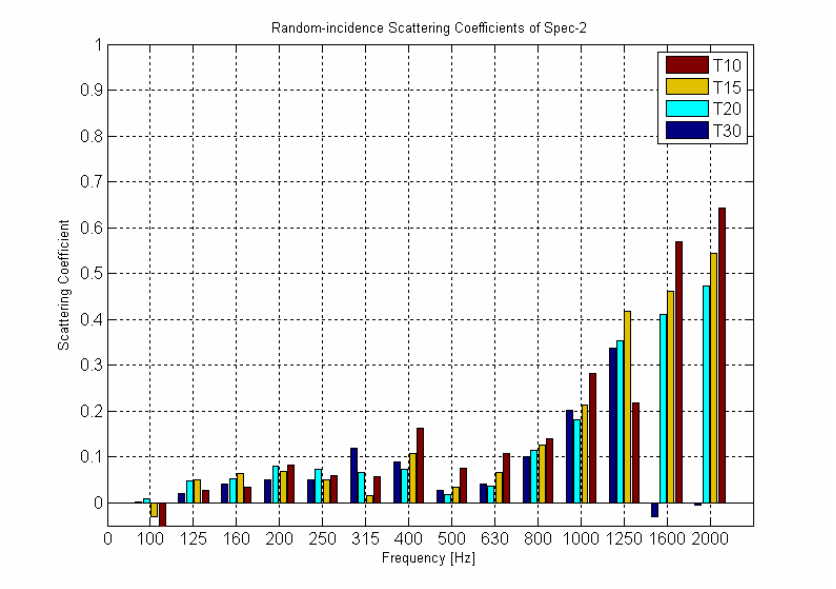

Figure D.3 – Random-incidence scattering coefficients of specimen 2 (Flush Mounting and ISO Method)

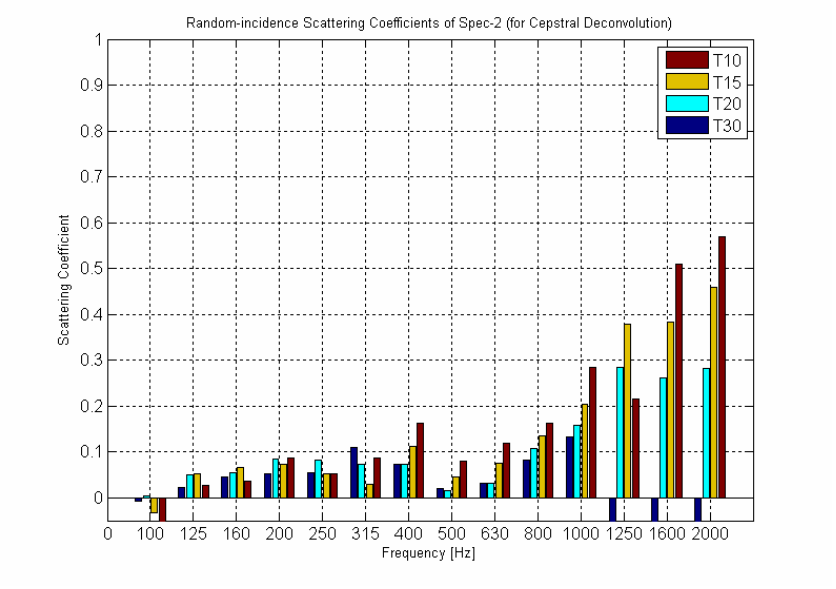

Figure D.4 – Random-incidence scattering coefficients of specimen 2 (Flush Mounting and Cepstral Deconvolution)

Table D.1 – Random-incidence absorption and scattering coefficients of the flush mounted specimen 2 and their uncertainties calculated according to both methods

Random-Incidence Absorption Coefficients for ISO Method

f (Hz)	100	125	160	200	250	315	400	500	630	800	1000	1250	1600	2000
T10	0,189	0,145	0,225	0,265	0,322	0,653	0,475	0,300	0,321	0,334	0,369	0,434	0,344	0,306
T20	0,194	0,143	0,161	0,225	0,325	0,578	0,483	0,329	0,319	0,373	0,443	0,469	0,358	0,337
T30	0,148	0,097	0,117	0,197	0,267	0,522	0,461	0,331	0,304	0,363	0,439	0,402	0,098	0,093
T15	0,201	0,148	0,185	0,270	0,329	0,614	0,473	0,318	0,334	0,346	0,419	0,472	0,347	0,302

Uncertainties in Absorption Coefficients for ISO Method

T10	0,058	0,073	0,034	0,040	0,049	0,041	0,038	0,046	0,054	0,060	0,075	0,095	0,113	0,114
T20	0,038	0,028	0,021	0,017	0,024	0,029	0,027	0,020	0,022	0,023	0,038	0,037	0,062	0,081
T30	0,027	0,021	0,023	0,015	0,029	0,018	0,019	0,015	0,018	0,018	0,027	0,107	0,172	0,054
T15	0,033	0,034	0,023	0,033	0,038	0,029	0,031	0,036	0,035	0,037	0,035	0,045	0,076	0,086

Random-Incidence Absorption Coefficients for Cepstral Deconvolution Method

T10	0,189	0,145	0,225	0,264	0,321	0,649	0,471	0,296	0,317	0,322	0,358	0,422	0,329	0,290
T20	0,194	0,142	0,160	0,222	0,321	0,575	0,483	0,329	0,321	0,379	0,450	0,483	0,374	0,350
T30	0,147	0,095	0,114	0,193	0,265	0,525	0,464	0,335	0,309	0,367	0,443	0,392	0,112	0,097
T15	0,201	0,148	0,185	0,269	0,327	0,612	0,468	0,311	0,328	0,343	0,415	0,474	0,345	0,303

Uncertainties in Absorption Coefficients for Cepstral Deconvolution Method

T10	0,058	0,073	0,034	0,040	0,050	0,044	0,042	0,050	0,058	0,068	0,087	0,105	0,129	0,127
T20	0,038	0,028	0,022	0,019	0,027	0,031	0,028	0,020	0,021	0,019	0,036	0,031	0,050	0,073
T30	0,028	0,022	0,024	0,017	0,030	0,016	0,018	0,013	0,015	0,016	0,025	0,120	0,169	0,055
T15	0,033	0,034	0,024	0,034	0,039	0,032	0,036	0,042	0,041	0,040	0,039	0,045	0,081	0,087

Random-Incidence Scattering Coefficients for ISO Method

f (Hz)	100	125	160	200	250	315	400	500	630	800	1000	1250	1600	2000
T10	-0,066	0,027	0,034	0,083	0,059	0,057	0,163	0,074	0,107	0,140	0,283	0,218	0,570	0,643
T20	0,009	0,049	0,052	0,080	0,074	0,065	0,074	0,017	0,035	0,114	0,182	0,353	0,411	0,473
T30	0,001	0,021	0,041	0,049	0,051	0,119	0,089	0,027	0,041	0,101	0,202	0,337	-0,031	-0,006
T15	-0,030	0,051	0,063	0,069	0,049	0,016	0,108	0,034	0,065	0,126	0,213	0,417	0,461	0,544

Uncertainties in Scattering Coefficients for ISO Method

T10	0,098	0,104	0,058	0,074	0,102	0,189	0,081	0,075	0,102	0,106	0,145	0,215	0,144	0,132
T20	0,071	0,040	0,028	0,029	0,037	0,091	0,057	0,035	0,037	0,039	0,062	0,071	0,069	0,089
T30	0,045	0,030	0,032	0,025	0,057	0,062	0,039	0,026	0,029	0,029	0,049	0,276	0,267	0,094
T15	0,067	0,045	0,032	0,057	0,074	0,114	0,061	0,061	0,063	0,069	0,080	0,098	0,104	0,092

Random-Incidence Scattering Coefficients for Cepstral Deconvolution Method

T10	-0,066	0,028	0,035	0,088	0,052	0,087	0,161	0,079	0,118	0,163	0,285	0,214	0,510	0,570
T20	0,005	0,050	0,055	0,084	0,082	0,074	0,072	0,016	0,033	0,107	0,157	0,285	0,262	0,283
T30	-0,009	0,022	0,046	0,053	0,055	0,110	0,073	0,021	0,032	0,082	0,133	-0,164	-0,692	-0,448
T15	-0,032	0,052	0,067	0,073	0,051	0,030	0,112	0,046	0,075	0,134	0,204	0,378	0,383	0,459

Uncertainties in Scattering Coefficients for Cepstral Deconvolution Method

T10	0,098	0,104	0,059	0,074	0,099	0,195	0,089	0,079	0,106	0,112	0,150	0,205	0,138	0,139
T20	0,071	0,040	0,029	0,032	0,041	0,094	0,057	0,034	0,036	0,034	0,060	0,065	0,069	0,095
T30	0,046	0,031	0,033	0,027	0,056	0,061	0,039	0,023	0,025	0,029	0,049	0,387	0,334	0,110
T15	0,067	0,044	0,033	0,058	0,075	0,116	0,067	0,066	0,070	0,071	0,081	0,090	0,111	0,090